

Metabolic regulation of gene expression by histone lactylation

<https://doi.org/10.1038/s41586-019-1678-1>

Received: 21 June 2018

Accepted: 13 September 2019

Published online: 23 October 2019

Di Zhang^{1,12}, Zhanyun Tang^{2,12}, He Huang^{1,9}, Guolin Zhou¹, Chang Cui¹, Yeting Weng¹, Wenchao Liu¹, Sunjoo Kim³, Sangkyu Lee³, Mathew Perez-Neut¹, Jun Ding¹, Daniel Czyz⁴, Rong Hu^{5,6}, Zhen Ye^{5,6}, Maomao He⁷, Y. George Zheng⁷, Howard A. Shuman⁴, Lunzhi Dai^{1,10}, Bing Ren^{5,6}, Robert G. Roeder², Lev Becker^{1,8,11*} & Yingming Zhao^{1,8*}

The Warburg effect, which originally described increased production of lactate in cancer, is associated with diverse cellular processes such as angiogenesis, hypoxia, polarization of macrophages and activation of T cells. This phenomenon is intimately linked to several diseases including neoplasia, sepsis and autoimmune diseases^{1,2}. Lactate, which is converted from pyruvate in tumour cells, is widely known as an energy source and metabolic by-product. However, its non-metabolic functions in physiology and disease remain unknown. Here we show that lactate-derived lactylation of histone lysine residues serves as an epigenetic modification that directly stimulates gene transcription from chromatin. We identify 28 lactylation sites on core histones in human and mouse cells. Hypoxia and bacterial challenges induce the production of lactate by glycolysis, and this acts as a precursor that stimulates histone lactylation. Using M1 macrophages that have been exposed to bacteria as a model system, we show that histone lactylation has different temporal dynamics from acetylation. In the late phase of M1 macrophage polarization, increased histone lactylation induces homeostatic genes that are involved in wound healing, including *Arg1*. Collectively, our results suggest that an endogenous 'lactate clock' in bacterially challenged M1 macrophages turns on gene expression to promote homeostasis. Histone lactylation thus represents an opportunity to improve our understanding of the functions of lactate and its role in diverse pathophysiological conditions, including infection and cancer.

Inspired by the discovery of various histone acylations derived from cellular metabolites^{3,4}, we predicted and identified lysine lactylation (Kla) as a new type of histone mark that can be stimulated by lactate (Fig. 1a). Initial evidence for histone Kla came from the observation of a mass shift of 72.021 Da on lysine residues in three proteolytic peptides that were detected in high-performance liquid chromatography (HPLC)–tandem mass spectrometry (MS/MS) analysis of tryptically digested core histones from human MCF-7 cells (Fig. 1b and Extended Data Fig. 1b, d). This mass shift is the same as that caused by the addition of a lactyl group to the ε-amino group of a lysine residue.

To validate the existence of lysine lactylation in histones, we used four orthogonal methods⁵. In the first two methods, we used HPLC–MS/MS analysis to compare a synthetic peptide with its in vivo-derived counterpart to determine whether the two versions of the peptide have the same chemical properties in terms of chromatographic elution in HPLC analysis and fragmentation pattern in MS/MS analysis. To achieve this,

we generated three histone peptides bearing Kla modifications: H3K23-QLATK_{la}AAR; H2BK5-PELAK_{la}SAPAK; and H4K8-GGK_{la}GLGK. Each pair of peptides co-eluted in HPLC and had comparable MS/MS spectra (Fig. 1b and Extended Data Fig. 1a–e). To confirm the modification further, we developed a pan anti-Kla antibody (Extended Data Fig. 1f, g). Immunoblots using the pan anti-Kla antibody confirmed the presence of histone Kla and showed that histone Kla levels were increased in a dose-dependent fashion in response to exogenous L-lactate (Extended Data Fig. 1h–j). Subsequent mass spectrometry analyses identified 26 and 16 histone Kla sites from human HeLa cells and mouse bone marrow-derived macrophages (BMDMs), respectively (Fig. 1c). Finally, metabolic labelling experiments using isotopic sodium L-lactate (¹³C₃) followed by MS/MS analysis demonstrated that lysine lactylation can be derived from lactate (Extended Data Fig. 1k). Together, these experiments demonstrate that histone Kla is an in vivo protein post-translational modification derived from lactate.

¹Ben May Department for Cancer Research, The University of Chicago, Chicago, IL, USA. ²Laboratory of Biochemistry and Molecular Biology, The Rockefeller University, New York, NY, USA.

³BK21 Plus KNU Multi-Omics based Creative Drug Research Team, College of Pharmacy, Research Institute of Pharmaceutical Sciences, Kyungpook National University, Daegu, South Korea.

⁴Department of Microbiology, The University of Chicago, Chicago, IL, USA. ⁵Ludwig Institute for Cancer Research, University of California at San Diego, La Jolla, CA, USA. ⁶Center for Epigenomics and Department of Cellular and Molecular Medicine, University of California, San Diego School of Medicine, La Jolla, CA, USA. ⁷Department of Pharmaceutical and Biomedical Sciences, University of Georgia, Athens, GA, USA. ⁸University of Chicago Medicine Comprehensive Cancer Center, Chicago, IL, USA. ⁹Present address: Shanghai Institute of Materia Medica, Chinese Academy of Sciences, Shanghai, China. ¹⁰Present address: Department of General Practice, State Key Laboratory of Biotherapy, West China Hospital, Sichuan University, and Collaborative Innovation Center of Biotherapy, Chengdu, China. ¹¹Ludwig Center for Metastasis Research, The University of Chicago, Chicago, IL, USA. ¹²These authors contributed equally: Di Zhang, Zhanyun Tang. *e-mail: levb@uchicago.edu; yingming.zhao@uchicago.edu

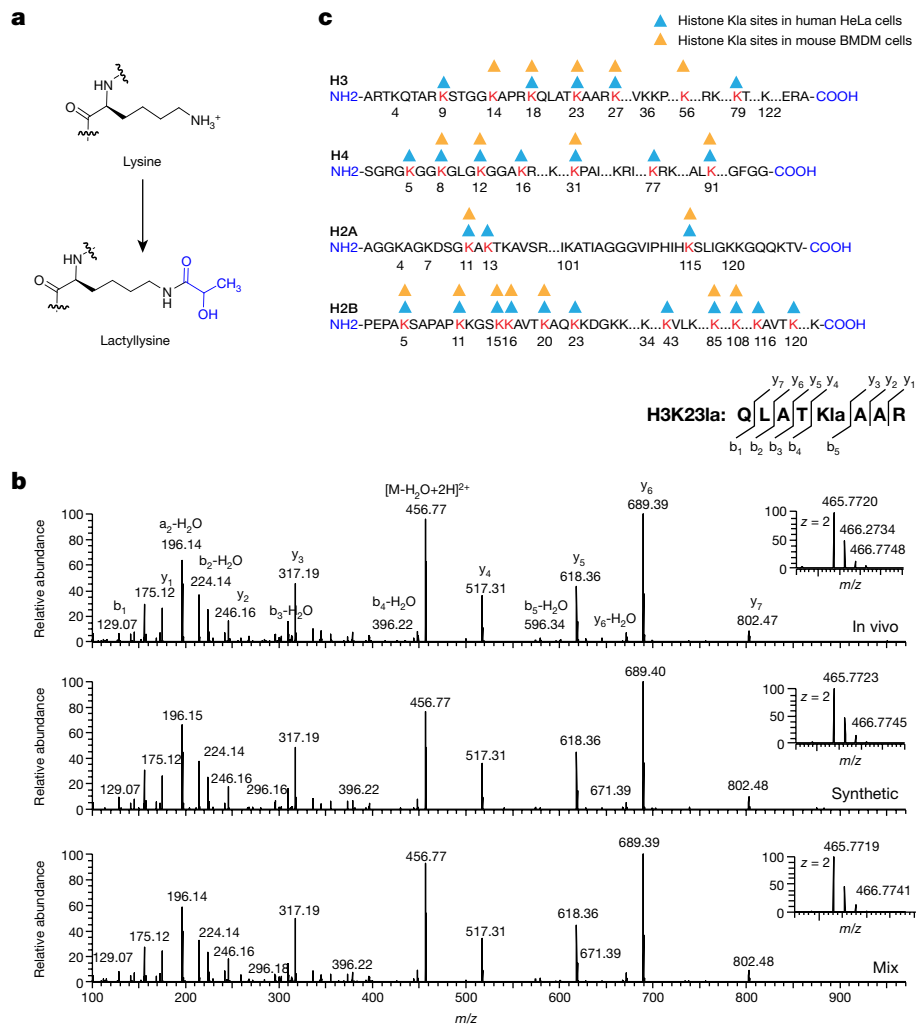


Fig. 1 | Identification and validation of histone Kla. **a**, Illustration of Kla structure. **b**, MS/MS spectra of a lactylated histone peptide (H3K23la) derived from MCF-7 cells (*in vivo*), its synthetic counterpart, and their mixture. The *b* ion

refers to the N-terminal parts of the peptide, and the *y* ion refers to the C-terminal parts of the peptide. Data represent two independent experiments. **c**, Illustration of histone Kla sites identified in human and mouse cells.

Histone Kla is regulated by glycolysis

Given that extracellular lactate can stimulate histone Kla, we hypothesized that modulation of intracellular lactate production would also affect histone Kla levels. We exposed MCF-7 and other cell lines to various concentrations of glucose, the major source of intracellular lactate. Both lactate production and histone Kla levels were induced by glucose in a dose-dependent manner (Fig. 2a, b and Extended Data Fig. 2a–c). Conversely, the non-metabolizable glucose analogue 2-deoxy-D-glucose (2-DG) decreased both lactate production and histone Kla levels (Fig. 2c, d). Furthermore, metabolic labelling experiments using isotopic glucose ($U^{-13}\text{C}_6$) followed by MS/MS analysis demonstrated that lysine lactylation is endogenously derived from glucose (Extended Data Fig. 2d and Supplementary Table 1). Quantitative proteomics analysis across a diverse set of histone sites demonstrated that histone Kla and Kac have different kinetics of $U^{-13}\text{C}_6$ -glucose incorporation in MCF-7 cells (Extended Data Fig. 2e, f). ^{13}C -labelled histone Kac reached a steady state at 6 h—similar to the previous observation in HCT116 cells⁶. By contrast, histone Kla increased over a 24-h time course (Extended Data Fig. 2e, f). Immunoblotting results corroborated the MS/MS data in cell lines such as MCF-7 cells (Extended Data Fig. 2i–k).

Lactate production is determined by the balance between glycolysis and mitochondrial metabolism. We tested whether the activities of enzymes in these two pathways can modulate lactate levels that in turn

regulate histone Kla (Fig. 2e). Sodium dichloroacetate (DCA) and oxamate were used to inhibit lactate production by modulating the activities of pyruvate dehydrogenase and lactate dehydrogenase, respectively. As anticipated, intracellular levels of lactate were decreased by these two compounds (Fig. 2f) and levels of histone Kla were lowered (Fig. 2g, h). By contrast, rotenone—an inhibitor of the mitochondrial respiratory chain complex I that drives cells towards glycolysis—increased levels of both intracellular lactate and histone Kla (Fig. 2f, i). Quantification of histone Kla and Kac marks by stable isotope labelling with amino acids in cell culture (SILAC) and MS/MS analyses corroborated the immunoblot data from DCA- and rotenone-treated MCF-7 cells (Extended Data Fig. 2l, m). Furthermore, labelling experiments with $U^{-13}\text{C}_6$ -glucose showed that the incorporation of ^{13}C into histone Kla but not Kac was decreased by DCA (Extended Data Fig. 2e–h). Together, these observations demonstrate that endogenous production of lactate is a key determinant of histone Kla levels.

Hypoxia and bacterial exposure stimulate histone Kla

Increased glycolysis and lactate production are coupled with diverse cellular processes. To investigate whether histone Kla is regulated by glycolysis under physiological conditions, we chose two model systems: hypoxia and M1 macrophage polarization. In response to hypoxia, cells reprogram their metabolism by inhibiting oxidative phosphorylation

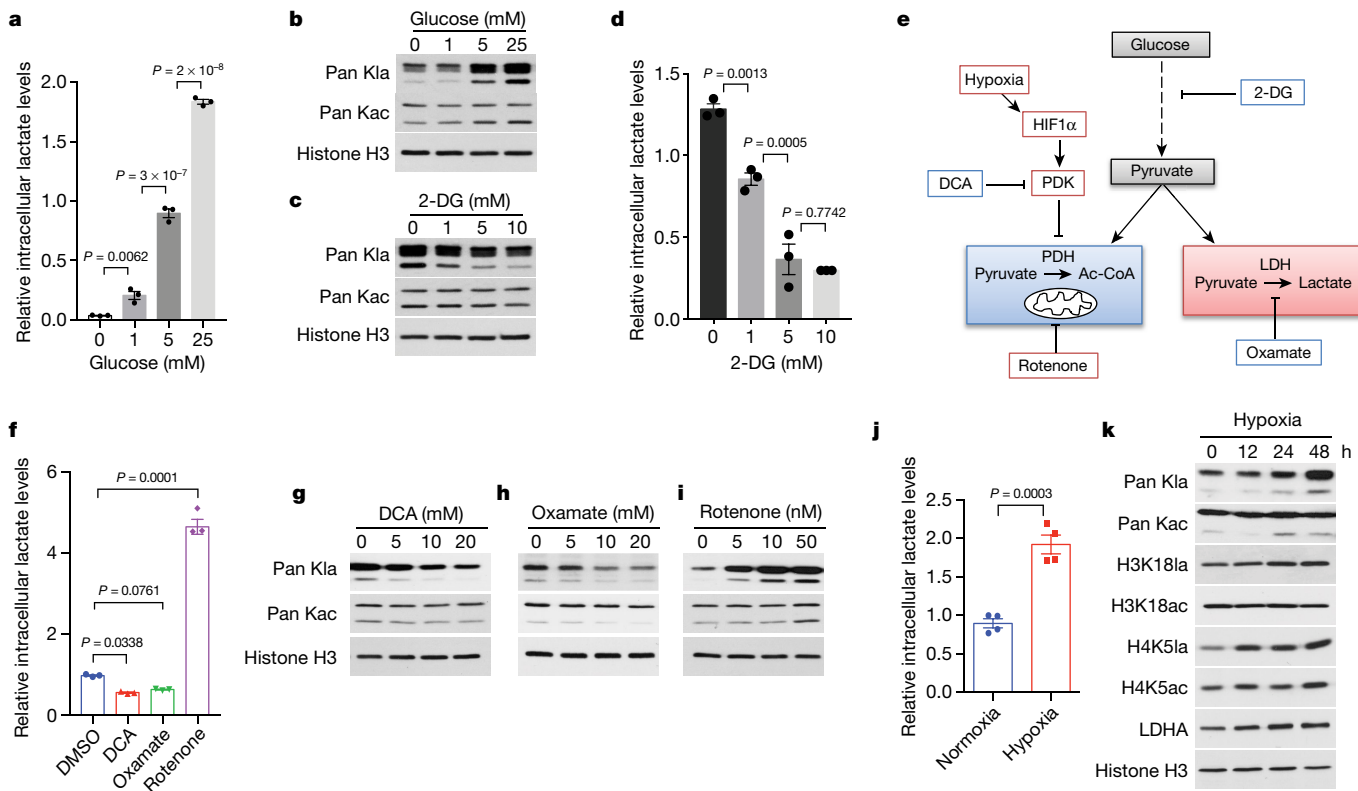


Fig. 2 | Lactate regulates histone Kla. **a–d**, Intracellular lactate levels (**a**, **d**) and histone Kla levels (**b**, **c**) were measured from MCF-7 cells cultured in different concentrations of glucose or 2-DG in the presence of 25 mM glucose for 24 h. Lactate was measured by a lactate colorimetric kit. $n=3$ biological replicates; statistical significance was determined using one-way ANOVA followed by Sidak's multiple comparisons test. Immunoblots were performed using acid-extracted histone samples. The pan anti-Kla and anti-Kac immunoblots indicate molecular masses between 10 and 15 kDa. **e**, Regulation of glycolysis and lactate production by diverse metabolic modulators. **f**, Intracellular lactate levels were measured in MCF-7 cells treated with indicated glycolysis modulators for 24 h.

$n=3$ biological replicates; statistical significance was determined using one-way ANOVA followed by Dunnett's multiple comparisons test. **g–i**, Immunoblots of acid-extracted histones (rotenone and DCA) or whole-cell lysates (oxamate) from MCF-7 cells in response to different glycolysis modulators. **j**, Intracellular lactate levels were measured in MCF-7 cells in response to hypoxia. $n=4$ biological replicates; statistical significance was determined using unpaired two-tailed *t*-test. **k**, Immunoblots of acid-extracted histones from MCF-7 cells under hypoxia (1% oxygen) for indicated time points. Data in **a**, **d**, **f** and **j** are mean and s.e.m. Data in **b**, **c**, **g**–**i** and **k** represent three independent experiments.

and enhancing glycolysis, which stimulates the production of lactate⁷. Hypoxia induced intracellular production of lactate and increased histone Kla levels but not Kac levels in MCF-7 cells (Fig. 2j, k and Extended Data Fig. 3a–d). SILAC-based mass spectrometric quantification of histone Kla and Kac confirmed the immunoblotting data (Extended Data Fig. 3e, f). Similar results were obtained in HeLa and RAW 264.7 cells (Extended Data Fig. 3g, h). Furthermore, we found that the induction of lactate production and histone Kla by hypoxia was attenuated by a lactate dehydrogenase inhibitor (oxamate) or a PDK1 inhibitor (DCA) (Extended Data Fig. 3i, j). Deletion of both LDHA and LDHB fully suppressed production of lactate and histone Kla in HepG2 cells under normoxic conditions (Extended Data Fig. 3k, l). Owing to poor cell viability, hypoxic conditions could not be tested (data not shown).

Emerging evidence shows that lactate has regulatory functions in both innate and adaptive immune cells⁸ and induces marked changes in gene expression⁹, suggesting that lactate is not simply a ‘waste product’ of glycolysis. Pro-inflammatory M1 macrophages undergo metabolic reprogramming towards aerobic glycolysis, resulting in lactate production, whereas anti-inflammatory M2 macrophages trigger a metabolic program of increased oxidative phosphorylation and fatty acid oxidation¹⁰. Our discovery of histone Kla marks and their dynamics therefore suggests a role in regulating gene expression during M1 macrophage polarization.

To test this hypothesis, we examined the dynamics of lactate production and histone Kla marks during M1 macrophage polarization after

treatment of BMDMs with lipopolysaccharide (LPS) and interferon-γ (IFNγ). We observed increased intracellular lactate levels 16–24 h after M1 activation (Fig. 3a), which correlated with increased histone Kla levels (Fig. 3b, c). By contrast, histone Kac levels were decreased at these time points (Fig. 3b, c). This differential pattern was confirmed by U-¹³C₆-glucose labelling experiments, in which ¹³C-labelled histone Kac peaked 3 h after labelling and declined to a steady state, whereas histone Kla increased over the 24-h time course (Extended Data Fig. 4a–d). In addition, the LDHA-specific inhibitor GNE-140 reduced ¹³C incorporation into histone Kla, but not Kac (Extended Data Fig. 4e, f). The increase of histone Kla during M1 polarization is intrinsic and not due to paracrine effects, because replenishing cells with fresh media every 4 h did not affect Kla levels (Extended Data Fig. 4g). Increases in lactate production and histone Kla are also specific to M1 macrophages because they were not observed in M2-polarized BMDMs (Fig. 3d and Extended Data Fig. 4h), which are more reliant on fatty acid oxidation¹⁰.

Histone Kla induces M2-like genes in M1 macrophages

Histone modifications have an important role in the regulation of gene expression¹¹. To investigate histone Kla-associated genes 24 h after M1 polarization of macrophages, we performed RNA sequencing (RNA-seq) and paired chromatin immunoprecipitation followed by sequencing (ChIP-seq) using anti-H3K18la or anti-H3K18ac antibodies (the specificities of which were validated by dot blots) (Extended Data Fig. 3a–d),

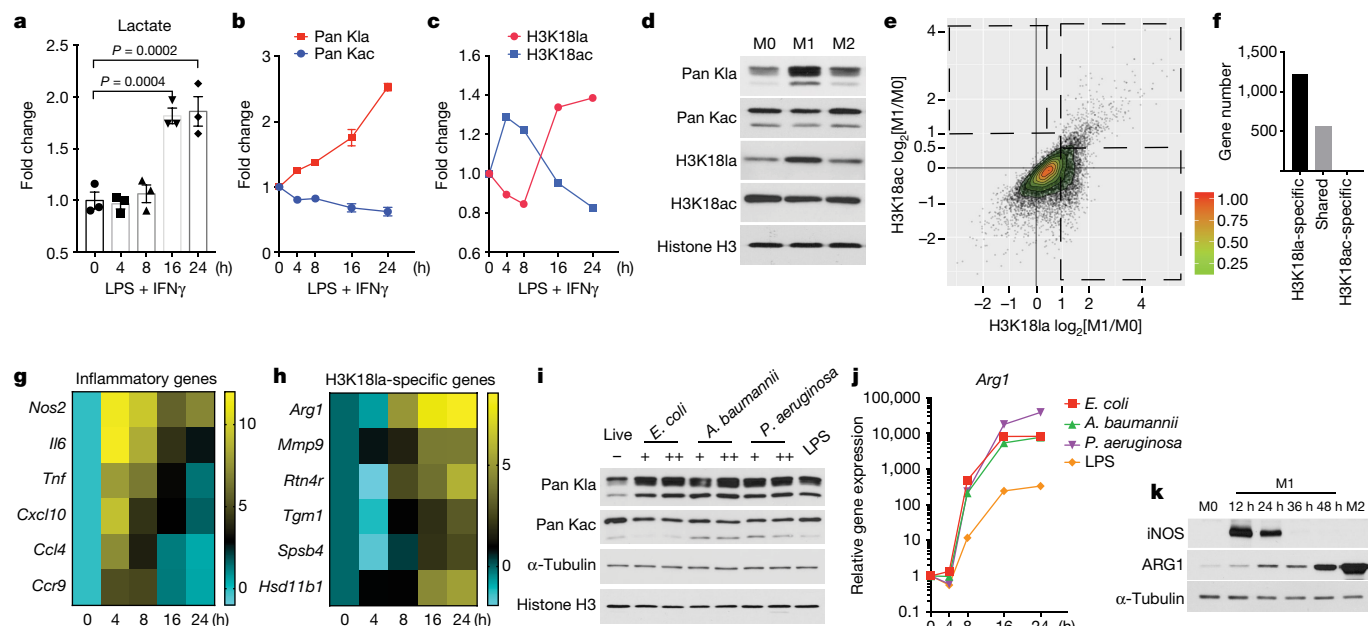


Fig. 3 | Increased histone Kla during M1 macrophage polarization is associated with M2-like gene activation. **a–c**, BMDMs were activated with LPS and IFN γ . *n* = 3 biological replicates; statistical significance was determined using one-way ANOVA followed by Dunnett's multiple comparisons test. **b, c**, Histone acylations were analysed by immunoblots using whole-cell lysates. ImageJ was used for quantification; *n* = 3 technical replicates. Data represent two independent experiments. **d**, BMDM cells were stimulated with PBS (M0), LPS and IFN γ (M1), and IL-4 (M2) for 24 h, respectively. Acid-extracted histones were used for immunoblots. **e, f**, Scatter plot (e) and bar plot (f) showing genes with promoters marked by exclusively increased H3K18la (H3K18la- $\log_2[M1/M0] \geq 1$ and H3K18ac- $\log_2[M1/M0] \leq 0.5$, H3K18la-specific); increased in both H3K18la and H3K18ac (H3K18la- $\log_2[M1/M0] \geq 1$ and H3K18ac- $\log_2[M1/M0] \geq 0.5$, shared); or exclusively increased H3K18ac (H3K18ac- $\log_2[M1/M0] \geq 1$, H3K18ac-specific). **g, h**, Heat maps showing gene expression kinetics (using reads per kilobase of transcript per million mapped reads (RPKM) values from RNA-seq) of exemplar inflammatory genes (g) and H3K18la-specific genes (h). The colour key represents \log_2 -transformed fold change relative to gene expression at 0 h. *n* = 4 biological replicates. **i, j**, BMDM cells were infected with indicated Gram-negative bacteria or LPS, respectively. **i**, Histone Kla levels were measured by immunoblot at 24 h after bacterial challenge. '+' indicates lower dose, and '++' indicates higher dose. **j**, Gene expression was analysed by quantitative PCR with reverse transcription (RT-qPCR) at indicated time points after bacterial challenge. *n* = 3 biological replicates. **k**, Protein levels of inducible nitric oxide synthase (iNOS) and ARG1 were analysed by immunoblots from BMDMs activated by the indicated stimuli. Data in **a–c, j** are mean and s.e.m. Data in **d, i** and **k** represent three independent experiments.

[M1/M0] ≥ 1 and H3K18la- $\log_2[M1/M0] \leq 0.5$, H3K18ac-specific). **g, h**, Heat maps showing gene expression kinetics (using reads per kilobase of transcript per million mapped reads (RPKM) values from RNA-seq) of exemplar inflammatory genes (g) and H3K18la-specific genes (h). The colour key represents \log_2 -transformed fold change relative to gene expression at 0 h. *n* = 4 biological replicates. **i, j**, BMDM cells were infected with indicated Gram-negative bacteria or LPS, respectively. **i**, Histone Kla levels were measured by immunoblot at 24 h after bacterial challenge. '+' indicates lower dose, and '++' indicates higher dose. **j**, Gene expression was analysed by quantitative PCR with reverse transcription (RT-qPCR) at indicated time points after bacterial challenge. *n* = 3 biological replicates. **k**, Protein levels of inducible nitric oxide synthase (iNOS) and ARG1 were analysed by immunoblots from BMDMs activated by the indicated stimuli. Data in **a–c, j** are mean and s.e.m. Data in **d, i** and **k** represent three independent experiments.

ChIP and quantitative PCR (qPCR) assays (Extended Data Fig. 4i, j) and immunoblots (Extended Data Fig. 4k).

Our ChIP-seq data showed that H3K18la and H3K18ac were both enriched in promoter regions (± 2 kb around transcriptional start sites) (Extended Data Fig. 4l) and were indicative of steady-state mRNA levels (Extended Data Fig. 4m, n). In addition, increased H3K18la (twofold increase) marked more genes than decreased H3K18la (twofold decrease), whereas the converse was true for the H3K18ac modification (Fig. 3e). Moreover, most genes marked by increased H3K18la were specific, because 68% of these genes (1,223 out of 1,787) did not display significantly increased H3K18ac (Fig. 3e, f and Supplementary Tables 2, 3). By contrast, no H3K18ac-specific genes were identified (Fig. 3e, f). Representative tracks from ChIP-seq studies are shown in Extended Data Fig. 4o, p.

To study correlations between H3K18la marks and gene expression, we performed RNA-seq analysis 0, 4, 8, 16 and 24 h after challenge with LPS and IFN γ (Extended Data Fig. 5a and Supplementary Table 4). As expected, inflammatory response genes (for example, *Nos2*) were induced as early as 4 h after challenge with LPS and IFN γ , and their expression levels steadily declined at later time points (Fig. 3g). Notably, the 1,223 genes specifically marked by increased H3K18la were more likely to be activated or reactivated at later time points (16 or 24 h) during M1 polarization (Fig. 3h and Extended Data Fig. 5a–c), which correlated well with the induction of intracellular lactate and histone Kla levels at these later time points (Fig. 3a–c). Gene Ontology (GO) analysis revealed that these H3K18la-specific genes were enriched in biological pathways that are independent of inflammation (Extended Data Fig. 5d). One of these

enriched pathways was wound healing (for example, *Arg1*), which has been associated with the M2-like phenotype (Fig. 3h and Extended Data Fig. 5d). To corroborate these findings with more physiologically relevant stimuli, we treated BMDMs (M0) with live or dead Gram-negative bacteria (*Escherichia coli*, *Acinetobacter baumannii* and *Pseudomonas aeruginosa*) to stimulate M1 polarization. Similar to treatment with LPS, bacteria induced lactate production and global histone Kla but not histone Kac levels (Fig. 3i and Extended Data Fig. 5e, f), and the kinetics of early cytokine and late *Arg1* expression were maintained (Fig. 3j and Extended Data Fig. 5g–j).

Arginine metabolism is a key catabolic and anabolic process that is regulated during macrophage polarization. M1 macrophages are thought to have low levels of ARG1 and metabolize arginine via nitric oxide synthase to produce nitric oxide to kill pathogens, whereas M2 macrophages have high levels of ARG1, which produces ornithine to facilitate wound healing¹². Consistent with their RNA dynamics, ARG1 protein levels and activity were markedly increased 24–48 h after M1 polarization, whereas NOS2 protein levels and function peaked 12 h after M1 polarization and declined at later time points (Fig. 3k and Extended Data Fig. 5k). Collectively, these findings suggest that induction of lactate during M1 activation might promote a late-phase switch to a more homeostatic phenotype, which shares some similarity with the M2-like phenotype. Indeed, previous studies showed that treating BMDMs with lactate derived from tumour cells drives an M2-like phenotype that is characteristic of tumour-associated macrophages (TAMs)¹³. Using mouse cancer models, we observed a positive correlation between *Arg1* expression and histone Kla levels, but not histone Kac levels in TAMs

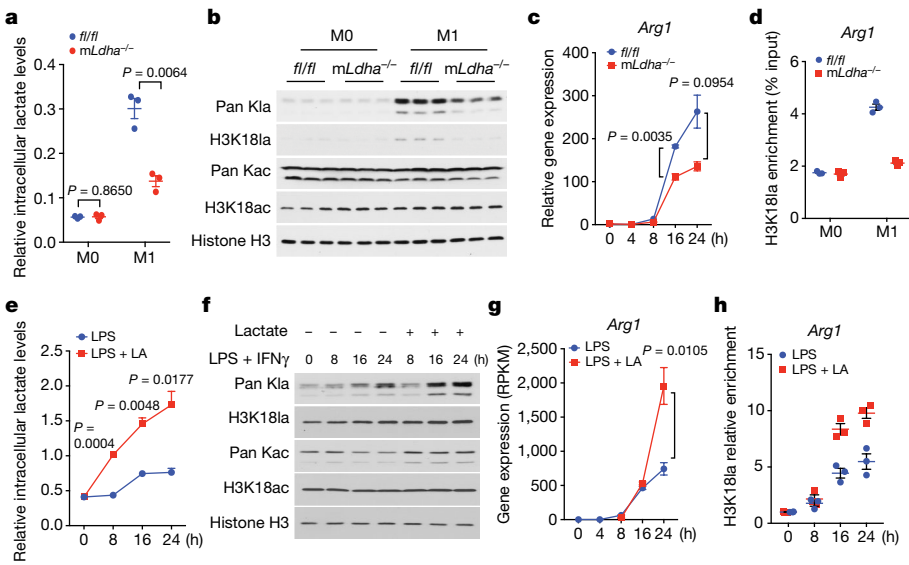


Fig. 4 | Lactate activates M2-like gene expression through histone K1a. **a–d**, Decreased lactate production in LDHA-deficient (myeloid-specific *Ldha*^{-/-}; *mLdha*^{-/-}) BMDM cells resulted in lowered histone K1a levels and *Arg1* expression during M1 polarization. *fl/fl*, littermate control mice. Intracellular lactate levels were measured using a lactate colorimetric kit (**a**) and global histone K1a levels were measured by immunoblots (**b**) 24 h after M1 polarization. **c**, Gene expression was analysed by RT-qPCR at indicated time points after M1 polarization. **a–c**, *n*=3 biological replicates. **d**, H3K18la occupancy was analysed by ChIP-qPCR 24 h after M1 polarization. Data represent three technical replicates from pooled samples. **e–h**, Exogenous lactic acid (LA) (25 mM) was

added to BMDM cells 4 h after M1 polarization (LPS + IFN γ), and cells were collected at indicated time points after M1 polarization for intracellular lactate measurement (**e**), histone K1a immunoblot analysis (**f**), gene expression analysis (**g**) and H3K18la occupancy analysis by ChIP-qPCR (**h**). **e**, *n*=3 biological replicates. **f**, Data represent three independent experiments. **g**, *n*=4 biological replicates. **h**, Data represent three technical replicates from pooled samples. Data in **a**, **c–e**, **g** and **h** are mean and s.e.m.; statistical significance was determined using multiple *t*-tests corrected using the Holm–Sidak method (**a**, **c**, **e**, **g**).

isolated from B16F10 melanoma and LLC1 lung tumours (Extended Data Fig. 6a–e).

Changes in gene expression during M1 polarization are caused by complex signalling cascades induced by LPS and IFN γ , including the induction of lactate and histone K1a. To substantiate the role of lactate and histone K1a in the regulation of gene expression, we manipulated levels of lactate during M1 polarization and examined its effect on the expression of *Arg1*, an M2-like gene. We first lowered lactate levels by deleting *Ldha* (*LysM-Cre*^{+/+}*Ldha*^{fl/fl}; Extended Data Fig. 7a–c). Lactate production and global histone K1a levels were both decreased in LDHA-deficient macrophages during M1 polarization (Fig. 4a, b). Although deleting *Ldha* in macrophages did not alter the expression of pro-inflammatory cytokines (Extended Data Fig. 7d–g), it attenuated *Arg1* and decreased histone K1a marks at the *Arg1* promoter (Fig. 4c, d). Similar findings were obtained when macrophages were M1 polarized in the presence of glycolysis inhibitors (2-DG, DCA and GNE-140) (Extended Data Fig. 7h–m). Next, we increased lactate levels by treating M1 macrophages with exogenous lactate. Exogenous lactate increased intracellular lactate (Fig. 4e) and histone K1a levels (Fig. 4f), and induced *Arg1* expression (Fig. 4g) and K1a levels at the *Arg1* promoter (Fig. 4h). By contrast, exogenous lactate did not affect the expression of early pro-inflammatory genes (Extended Data Fig. 8a–d). In addition, exogenous lactate enhanced the expression of other M2-like genes, such as *Vegfa* during M1 polarization (Extended Data Fig. 8e–h and Supplementary Table 5). Thus, these data confirmed the positive role of lactate and histone K1a in driving expression of M2-like genes during M1 macrophage polarization.

Histone K1a directly stimulates gene transcription

Our observed correlations between lactate, H3K18la and M2-like gene expression does not necessarily indicate that the histone K1a mark was a causative factor. Previous studies showed that exogenous lactate can alter *Arg1* and *Vegfa* expression in unstimulated (M0) macrophages by

HIF1 α ¹³. However, HIF1 α is unlikely to be important for regulating *Arg1* and *Vegfa* during M1 polarization as HIF1 α protein was induced at early time points and bound to promoters of glycolytic genes but not *Arg1* and *Vegfa* (Extended Data Fig. 8i–m).

To examine whether histone K1a has a direct role in transcriptional regulation, we took advantage of a cell-free, recombinant chromatin-templated histone modification and transcription assay (Extended Data Fig. 9a) that was used previously to demonstrate direct transcriptional activation by p53- and p300-dependent histone Kac¹⁴. This assay, in which acetyl-CoA was replaced by L-lactyl-CoA (validated by HPLC and mass spectrometry; Extended Data Fig. 9h–k), demonstrated robust p53-dependent, p300-mediated H3 and H4 lactylation (Extended Data Fig. 9b) and a corresponding effect on transcription (Extended Data Fig. 9c). The effects paralleled those observed for acetyl-CoA-dependent histone acetylation and transcription. To confirm that transcription was directly mediated by lactylation of histones, rather than other proteins in the nuclear extract, recombinant chromatin was reconstituted with core histones bearing lysine-to-arginine mutations in histone tails¹⁵. Compared with wild-type histones, the H3 and H4 mutations, but not the H2A or H2B mutations, eliminated p300- and p53-dependent transcription (Extended Data Fig. 9d). Together, these findings suggest that, similar to histone acetylation, histone lactylation can directly promote gene transcription under the described conditions. To examine the potential activity of p300 as a histone K1a writer in cells, we overexpressed p300 in HEK293T cells and observed a modest increase in histone K1a levels (Extended Data Fig. 9e). By contrast, p300 deletion in HCT116 and HEK293T cells decreased histone K1a levels (Extended Data Fig. 9f, g). Although we cannot exclude an indirect effect by p300 in these cells, together with the *in vitro* enzymatic results, these data suggest that p300 is a potential histone K1a writer protein.

In response to bacterial infection, macrophages must react rapidly with a substantial pro-inflammatory burst to help kill bacteria and recruit additional immune cells to the infection site. During this process,

macrophages switch to aerobic glycolysis¹⁰, which is thought to support pro-inflammatory cytokine expression during M1 activation¹⁶ and produce the Warburg effect. Over time, this metabolic switch also increases intracellular lactate, which we show stimulates histone lysine lactylation 16–24 h after exposure to M1-polarizing stimuli. Histone lactylation is not required for the induction or suppression of pro-inflammatory genes. Instead, it serves as a mechanism to initiate expression of homeostatic genes that have been traditionally associated with M2-like macrophages. Our studies support a model in which the switch to aerobic glycolysis that occurs during M1 polarization starts a ‘lactate timer’ that uses an epigenetic mechanism to induce M2-like characteristics in the late phase, perhaps to assist with repairing collateral damage incurred by the host during infection.

High levels of lactate (for example, 40 mM in certain type of tumour tissue¹⁷) is also associated with major hallmarks of diseases such as cancer. Given that the Kla modification can be stimulated by lactate and contribute to gene expression, the Kla modification is likely to fill an important knowledge gap in our understanding of diverse physiopathology (for example, infection, cancer) with which lactate is intimately associated.

Online content

Any methods, additional references, Nature Research reporting summaries, source data, extended data, supplementary information, acknowledgements, peer review information; details of author contributions and competing interests; and statements of data and code availability are available at <https://doi.org/10.1038/s41586-019-1678-1>.

- Pavlova, N. N. & Thompson, C. B. The emerging hallmarks of cancer metabolism. *Cell Metab.* **23**, 27–47 (2016).

- Palsson-McDermott, E. M. & O'Neill, L. A. The Warburg effect then and now: from cancer to inflammatory diseases. *BioEssays* **35**, 965–973 (2013).
- Sabari, B. R., Zhang, D., Allis, C. D. & Zhao, Y. Metabolic regulation of gene expression through histone acylations. *Nat. Rev. Mol. Cell Biol.* **18**, 90–101 (2017).
- Kaelin, W. G., Jr & McKnight, S. L. Influence of metabolism on epigenetics and disease. *Cell* **153**, 56–69 (2013).
- Tan, M. et al. Identification of 67 histone marks and histone lysine crotonylation as a new type of histone modification. *Cell* **146**, 1016–1028 (2011).
- Liu, X. et al. Acetate production from glucose and coupling to mitochondrial metabolism in mammals. *Cell* **175**, 502–513 (2018).
- Semenza, G. L. Oxygen sensing, hypoxia-inducible factors, and disease pathophysiology. *Annu. Rev. Pathol.* **9**, 47–71 (2014).
- Haas, R. et al. Intermediates of metabolism: from bystanders to signalling molecules. *Trends Biochem. Sci.* **41**, 460–471 (2016).
- Martinez-Outschoorn, U. E. et al. Ketones and lactate increase cancer cell “stemness,” driving recurrence, metastasis and poor clinical outcome in breast cancer: achieving personalized medicine via Metabolo-Genomics. *Cell Cycle* **10**, 1271–1286 (2011).
- Galván-Peña, S. & O'Neill, L. A. Metabolic reprogramming in macrophage polarization. *Front. Immunol.* **5**, 420 (2014).
- Allis, C. D. & Jenuwein, T. The molecular hallmarks of epigenetic control. *Nat. Rev. Genet.* **17**, 487–500 (2016).
- Rath, M., Müller, I., Kropf, P., Closs, E. I. & Munder, M. Metabolism via arginase or nitric oxide synthase: two competing arginine pathways in macrophages. *Front. Immunol.* **5**, 532 (2014).
- Colegio, O. R. et al. Functional polarization of tumour-associated macrophages by tumour-derived lactic acid. *Nature* **513**, 559–563 (2014).
- An, W., Kim, J. & Roeder, R. G. Ordered cooperative functions of PRMT1, p300, and CARM1 in transcriptional activation by p53. *Cell* **117**, 735–748 (2004).
- Tang, Z. et al. SET1 and p300 act synergistically, through coupled histone modifications, in transcriptional activation by p53. *Cell* **154**, 297–310 (2013).
- Tannahill, G. M. et al. Succinate is an inflammatory signal that induces IL-1 β through HIF-1 α . *Nature* **496**, 238–242 (2013).
- Walenta, S. et al. High lactate levels predict likelihood of metastases, tumor recurrence, and restricted patient survival in human cervical cancers. *Cancer Res.* **60**, 916–921 (2000).

Publisher's note Springer Nature remains neutral with regard to jurisdictional claims in published maps and institutional affiliations.

© The Author(s), under exclusive licence to Springer Nature Limited 2019

Methods

Materials

Pan anti-Kac (PTM-101), pan anti-Kla (PTM-1401), anti-H3K18la (PTM-1406), anti-H4K5la (PTM-1407) and anti-H4K8la (PTM-1405) antibodies were generated by PTM Bio Inc.; anti-histone H3 (ab12079), anti-H3K18ac (ab1191) and anti-H3K27ac (ab4729) antibodies were purchased from Abcam; *Drosophila* spike-in antibody (61686) and spike-in chromatin (53083) were obtained from Active Motif; anti-LDHA (2012S) antibody was from Cell Signaling Technology; anti- α -tubulin (05-829) and anti-LDHB (ABC927) antibodies were from Millipore Sigma; anti-HIF-1 α (NB100-105) antibody was from Novus Biologicals; anti-iNOS (GTX130246) and anti-ARG1 (GTX109242) antibodies were purchased from GeneTex; anti-p300 (sc-584) was from Santa Cruz Biotechnology; anti-CD11b monoclonal antibody (M1/70), PE-cyanine7 (25-0112-82) and anti-F4/80 monoclonal antibody (BM8), APC (17-4801-82) were from Thermo Fisher Scientific; lipopolysaccharides from *Escherichia coli* O111:B4 (L4391), sodium L-lactate (71718), L-(+)-lactic acid (L6402), sodium dichloroacetate (347795), cobalt (II) chloride hexahydrate (C8661), rotenone (R8875), and acetyl-CoA (A2056) were purchased from Sigma-Aldrich; sodium L-lactate (13C3, 98%) (CLM-1579-PK) and D-glucose (U-13C6, 99%) (CLM-1396-1) were purchased from Cambridge Isotope Laboratories. Recombinant mouse IFN γ protein (485-MI-100) was from R&D Systems; mouse IL-4 (130-097-760) was from Miltenyi Biotec; modified sequencing-grade trypsin was from Promega; lactate colorimetric assay kit II (K627-100), arginase activity colorimetric assay kit (K755-100), and nitric oxide synthase (NOS) activity assay kit (K205-100) were purchased from Biovision.

Cell culture

MCF-7, MDA-MB-231, HeLa, A549, HepG2, MEF and RAW 264.7 cells were obtained from the American Type Culture Collection and cultured in DMEM supplemented with 10% FBS and 1% GlutaMAX (GIBCO). Cells were routinely tested for mycoplasma contamination (MPO035, Sigma-Aldrich), and only negative cells were used in experiments. No specific cell line authentication was performed. For growth under hypoxic conditions, cells were grown in a specialized, humidified chamber equilibrated with 1% oxygen, 94% nitrogen, 5% carbon dioxide for the indicated time.

Mouse experiments

All animal use and experiments performed were approved by Institutional Animal Care and Use Committee (ACUP 72209) at the University of Chicago. *Ldha*^{fl/fl} mice (Jackson Laboratory, 030112) and LysM-Cre mice (Jackson Laboratory, 004781) were used to generate LysM-Cre^{+/+}*Ldha*^{fl/fl} and littermate control LysM-Cre^{−/−}*Ldha*^{fl/fl} mice. The following primers were used for genotyping: *Ldha* forward: CTGAGCACACCCATG TGAGA and *Ldha* reverse: AGCAACACTCCAAGTCAGGA. *LysM*-cre (*LysM* is also known as *Lyz2*): CCCAGAAATGCCAGATTACG, *LysM* common: CTTGGGCTGCCAGAATTCTC and *LysM* WT: TTACAGTCCGCCAGGC TGAC. Macrophages were derived from bone marrow of 8-week-old male C57BL/6 mice following the published procedure¹⁸. To induce an M1 or M2 phenotype, BMDM cells were stimulated with 5 ng ml^{−1} of LPS and 12 ng ml^{−1} of IFN γ , or 20 ng ml^{−1} of IL-4, for 24 h or the indicated time. To infect BMDM cells with bacteria, overnight cultures of *E. coli*, *A. baumannii* or *P. aeruginosa* were diluted in RPMI-1640 and added to BMDM cells in 6-well plates at 2 and 20 multiplicity of infection. A control plate was either infected with paraformaldehyde-killed bacteria or treated with 5 ng ml^{−1} LPS in the absence of bacteria. The plates were centrifuged at 975g for 30 min to promote infection, followed by a 30 min incubation in a humidified incubator at 37 °C at 5% CO₂. To kill extracellular bacteria, the medium overlying the confluent cell monolayer was replaced with fresh medium containing gentamicin at 100 µg ml^{−1} and the plates were further incubated for 1 h. After incubation, media were removed from infected cells and replaced with fresh media containing 25 µg ml^{−1} of gentamicin. For consistency, LPS-treated cells and cells infected with

dead bacteria were also treated with gentamicin. Cells were cultured for 24 h before lysis. Allocation of BMDM cells into different treated groups was randomized and not blinded.

Tumour inoculation and TAM isolation

LLC1 cells (0.5 × 10⁶) or B16F10 cells (1 × 10⁶) were injected into 7-week-old C57BL/6 mice (Jackson Laboratory). Once tumours reached approximately 600 mm³, mice were killed for tumour isolation. Tumours were digested with type 4 collagenase (Worthington, 3 mg ml^{−1}) and hyaluronidases (Sigma, 1.5 mg ml^{−1}) in 1% BSA/PBS at 37 °C with shaking at 200 r.p.m. for 30 min. The digested tumour was then filtered through a 70-µm cell strainer, followed by red blood cell lysis step and passing through another 40-µm strainer. Cells were resuspended into isolation buffer (0.1% BSA/PBS, 2 mM EDTA), layered onto Ficoll-Paque PLUS (GE Healthcare), and centrifuged at 450g for 30 min without a break. Mono-nuclear immune cells were obtained by taking out the middle white layer. TAMs were then isolated using CD11b Microbeads (Miltenyi Biotec) as the company instructed. The purity of TAMs purity was confirmed by flow cytometry using CD11b and F4/80 antibody. Data were quantified by FlowJo v.10.4.1.

Peptide immunoprecipitation

Histones from human MCF-7 or mouse BMDM cells were extracted using a standard acid-extraction protocol¹⁹, and subjected to trypsin digestion as per the manufacturer's instructions. Pan anti-Kla or pan anti-Kac antibodies were first conjugated to Protein A Sepharose beads (GE Healthcare BioSciences) and then incubated with tryptically digested histone peptides with gentle agitation overnight at 4 °C. The beads were then washed three times with NETN buffer (50 mM Tris-Cl pH 8.0, 100 mM NaCl, 1 mM EDTA, 0.5% NP-40), twice with ETN buffer (50 mM Tris-Cl pH 8.0, 100 mM NaCl, 1 mM EDTA) and once with water. Peptides were eluted from the beads with 0.1% TFA and dried in a SpeedVac system (Thermo Fisher Scientific).

HPLC-MS/MS analysis

The peptide samples were loaded onto a homemade capillary column (10 cm length × 75 mm ID, 3 µm particle size, Dr. Maisch GmbH) connected to an EASY-nLC 1000 system (Thermo Fisher Scientific). Peptides were separated and eluted with a gradient of 2% to 90% HPLC buffer B (0.1% formic acid in acetonitrile, v/v) in buffer A (0.1% formic acid in water, v/v) at a flow rate of 200 nL min^{−1} over 60 min (34 min for coelution studies). The eluted peptides were then ionized and analysed by a Q-Exactive mass spectrometer (Thermo Fisher Scientific). Full mass spectrometry was acquired in the Orbitrap mass analyser over the range *m/z* 300 to 1,400 with a resolution of 70,000 at *m/z* 200. The 12 most intense ions with charge ≥2 were fragmented with normalized collision energy of 27 and tandem mass spectra were acquired with a mass resolution of 17,500 at *m/z* 200.

Isotopic labelling experiments

MCF-7 cells were cultured in DMEM high-glucose media plus 10% FBS. To be labelled by isotopic lactate, cells were treated with 10 mM of ¹³C₃ sodium L-lactate for 24 h. To be labelled by isotopic glucose, cells were switched to DMEM No-Glucose media (Gibco) for 24 h, followed by supplementation with 25 mM of U-¹³C₆ D-glucose and continued culturing for three passages. Histones were extracted, digested with trypsin, immunoprecipitated using a pan anti-Kla antibody and analysed by HPLC-MS/MS as described above.

SILAC-based quantification

MCF-7 cells were cultured in either 'heavy' (L-Lys-¹³C₆, ¹⁵N₂) or 'light' (L-Lys-¹²C₆, ¹⁴N₂) DMEM, supplemented with 10% dialysed FBS (Serum Source International Inc.), for more than six passages, to achieve more than 99% labelling efficiency. Heavy-labelled and light-labelled cells were mixed in a 1:1 ratio. Histones were extracted, digested with trypsin,

Article

immunoprecipitated using a pan anti-Kla antibody, and analysed by HPLC–MS/MS as described above. Quantification was analysed by Maxquant²⁰. Ratio H/L derived from Maxquant was then normalized by protein abundance.

Synthesis of L-lactyl-CoA

L-Lactic acid (90 mg, 1 mmol) was dissolved in 5 ml of freshly distilled CH₂Cl₂, N-hydroxysuccinimide (115 mg, 1 mmol) was added to this solution, and the reaction mixture was sonicated to obtain a clear solution. Then, N,N'-dicyclohexylcarbodiimide (DCC, 227 mg, 1.1 mmol) was added. A white precipitate formed after addition. The reaction mixture was stirred at room temperature overnight. Then the white precipitate was filtered and washed with CH₃CN. The resulting organic solvent was evaporated by vacuum to afford crude product L-lactyl-NHS (170 mg, 91% yield), which was used in the next step without further purification. CoA hydrate (0.0065 mmol; 5 mg) was dissolved in 1.5 ml of 0.5 M NaHCO₃ (pH 8.0) and cooled down on ice bath. Then, L-lactyl-NHS (2.5 mg, 0.013 mmol) in 0.5 ml of CH₃CN/acetone (1:1 v/v) was added dropwise to the CoA solution. The reaction solution was stirred at 4 °C overnight and then quenched by adjusting pH to 4.0 with 1.0 M HCl. The reaction mixture was then subjected to RP-HPLC purification with gradient 5–45% buffer A in buffer B over 30 min at flow rate 5 ml min⁻¹; UV detection wavelength was fixed at 214 and 254 nm (HPLC buffer A: 0.05% TFA in water; HPLC buffer B: 0.05% TFA in acetonitrile). The fractions were collected and lyophilized after flash-freeze with liquid nitrogen. m = 2 mg, yield 38% ¹H NMR (400 MHz, Deuterium oxide) δ 8.57 (s, 1H), 8.33 (s, 1H), 6.12 (d, J = 5.7 Hz, 1H), 4.49 (s, 1H), 4.29 – 4.24 (m, 1H), 4.14 (s, 2H), 3.93 (s, 1H), 3.75 (d, J = 8.6 Hz, 1H), 3.48 (d, J = 7.6 Hz, 1H), 3.35 (t, J = 6.4 Hz, 2H), 3.22 (d, J = 5.2 Hz, 3H), 2.89 (q, J = 6.2 Hz, 2H), 2.32 (t, J = 6.4 Hz, 2H), 1.23 (d, J = 6.9 Hz, 3H), 0.83 (s, 3H), 0.70 (s, 3H). MALDI m/z calculated for C₂₄H₄₁N₇O₁₈P₃S⁺ [M + H]⁺: 840.1, found 839.6.

In vitro chromatin template-based histone modification and transcription assays

Purification of recombinant proteins and chromatin assembly were performed as previously described¹⁵. The chromatin-templated histone modification and transcription assays were as described previously¹⁵, except that lactyl-CoA was used in place of acetyl-CoA and [α -³²P]CTP was used in place of [α -³²P]UTP. The H3KR, H4KR, H2AKR and H2BKR histone mutants were the same as previously described¹⁵. Histone modifications were monitored by immunoblot and transcription products were monitored by autoradiography as described¹⁵.

RNA-seq

Total RNA was extracted from BMDM cells activated as indicated using a RNeasy Plus Mini Kit (74134, Qiagen). Two to four micrograms of total RNA were used as starting material to prepare libraries using Illumina TruSeq Stranded mRNA Library Prep Kit Set A (RS-122-2101, Illumina). The size of the libraries was selected by using the Agencourt AMPure XP beads (A63882, Beckman Coulter), with average size of 400 bp. The libraries were sequenced using Illumina HiSeq 4000 (pair end 50 bp).

Bioinformatic analysis of RNA-seq data: sequencing quality was evaluated by FastQC v.0.11.4. All reads were mapped to the reference genome of Illumina iGenomes UCSC mm10 using HISAT2 v.2.1.0²¹. Differential expression analysis was implemented using edgeR v.3.16.5²², after retaining only genes for which counts per million (cpm) was larger than one in four samples and normalizing the library sizes across samples using the TMM method of the edgeR package. Hierarchical clustering was performed and heat maps were generated using Perseus v.1.6.1.1 (<http://www.coxdocs.org/doku.php?id=perseus:start>). The log₂-transformed gene expression values (RPKM) were normalized by subtracting the mean in every row, and hierarchically clustered with a Pearson correlation algorithm. Gene Ontology analysis (GOTERM_BP_DIRECT) was carried out using DAVID bioinformatics resources 6.8^{23,24}.

The following primers were used for RT-qPCR analysis: Arg1: CTCCAGGCCAAAGTCCTTAGAG, AGGAGCTGTCAATTAGGGACATC; Vegfa: CCACGACAGAAGGAGAGCAGAAGTCC, CGTTACAGCAGCCTGCACAGCG; Il6: GTTCTCTGGAAATCGTGA, TTCTGCAACTGCATCATCG; Il1b: TTTGACAGTGATGAGAATGACC, CTCTGTTGATGTCTGCTGCTG; Ifnb1: CAGCTCCAAGAAAGGACGAAC, GGCAGTGTAACTCTTCATC; Cxcl10: CCAAGTGCTGCCCTCATTTTC, GGCTCGCAGGGATGATTCAA; Tnfa: CCCTCACACTCAGATCATCTTCT, GCTACGACGTGGCTACAG; and Rn18s (18S rRNA): GTAACCCGTTGAACCCCATT, CCATCCAATCGTAGTCG.

ChIP-seq

Native ChIP was carried out following the published protocol²⁵ with spike-in for normalization purpose. Spike-in was carried out according to vendor protocols (61686, Active Motif). In brief, 50 ng of Spike-in chromatin (53083, Active Motif) was added to 25 µg of BMDM chromatin to incubate with 2 µg Spike-in antibody (61686, Active Motif) together with 4 µg of anti-H3K18la or anti-H3K18ac antibodies. After 4 h of incubation at 4 °C, Protein A Sepharose (17-5280-01, GE Healthcare Life Sciences) was added and incubated for another 2 h, followed by sequential wash with buffer TSE I (0.1% SDS, 1% Triton X-100, 2 mM EDTA, 20 mM Tris-HCl pH 8.0, 150 mM NaCl), TSE II (0.1% SDS, 1% Triton X-100, 2 mM EDTA, 20 mM Tris-HCl pH 8.0, 500 mM NaCl), buffer III (0.25 M LiCl, 1% NP-40, 1% deoxycholate, 1 mM EDTA, 10 mM Tris-HCl pH 8.0), and TE buffer (1 mM EDTA, 10 mM Tris-HCl pH 8.0). Chromatin DNA was finally eluted with buffer containing 1% SDS and 0.1 M NaHCO₃. The eluates were digested with RNase A (12091021, Thermo Fisher Scientific) and proteinase K (AM2546, Thermo Fisher Scientific). DNA was recovered using the QIAquick PCR purification kit (28106, Qiagen) according to the manufacturer's instructions.

ChIP-seq libraries were constructed with an Accel-NGS 2S Plus DNA Library Kit (Swift Biosciences) according to the manufacturer's protocol. The libraries were then amplified and assessed for fragment size using TapeStation (Agilent) and quantified using a Qubit dsDNA HS Assay Kit (Thermo Fisher Scientific). The indexed libraries were pooled and sequenced on a Hiseq4000 Sequencer (Illumina) using the 50-nucleotide single-read configuration.

Bioinformatics analysis of ChIP-seq data: sequencing quality was evaluated by FastQC v.0.11.4. All reads were mapped to the reference genome of Illumina iGenomes UCSC mm10 using Bowtie v.2.2.6^{26,27}, and only uniquely mapped reads were retained. Then SAMtools v.0.1.19²⁸ was used to convert files to bam format, sort, and remove PCR duplicates. Peaks were called using MACS v.2.2.1²⁹ under q = 0.01. To quantify and directly compare H3K18la or H3K18ac in different samples (M0 and M1 macrophages), the uniquely mapped H3K18la or H3K18ac reads in promoter regions (\pm 2 kb around transcriptional start sites) of each gene were counted by featureCounts v.1.5.0-p1³⁰, and then normalized by Spike-in ChIP read counts of the corresponding condition (M0 or M1 macrophages). The overlap genes in ChIP-seq and RNA-seq data were used for all subsequent analysis. Gene Ontology analysis (GOTERM_BP_DIRECT) was carried out using DAVID Bioinformatics Resources 6.8^{23,24}.

The following primers were used for qPCR analysis of gene promoter regions in human cells: FOXO3 (previously known as FOXO3A) promoter: CAGTGAGTGTGCAGCTTG, AAAGCCTCCTGTTGTCCT; FOXO3 downstream: TGACACAGAACGCCAGAAG, GCTCCCCAAGAGACCTAA; LDHA promoter: TAAGGGTGGGGATACCTCT, CCCAAGAGAAAAATGCAAGC. The following primers were used for qPCR analysis of gene promoter regions in mouse cells: Arg1/Arg1-PTM: AAGCTGTGGCCTCAGAACAT, GGTAAACCGCTGTGAAAGGAT; Arg1-HRE-1kb: CCCGACTTTGACCCGAAGAA, CTTTACACAGGGACC GGACC; Arg1-HRE-2kb: TGTCTCTCCCAGTTCCCCA, AGCAACTTGGCATCTGATGGA; Vegfa/Vegfa-PTM: CGAGCTAGCACTCTCCAG, AACTTCTGGGCTCTCTCGC; Vegfa-HRE-1kb: GGCACCAAAATTGTCGGCACT, CTGCCAGACTACACAGTGA; Vegfa-HRE-2kb: ACCTGATCC TGATCCCTGCT, CAGCCTCTGTTATGCCACGA; Vegfa-HRE-3kb: CGACAACCTAGGCTTCACGT, TTGAAAGGGCTGACATGGCT; Eno1:

AAGGTCATCAGCAAGGTCGT, CGTACTCCGAGTCTCACACG; *Glut1* (also known as *Slc2a1*): TAGATCCCCTCCCTTTGCT, GAACACGTAGCCTGC TCACA; gene desert: CTGCCAGGGTTGTAGAGAGG, GCCAGATCATATT GGCTTGG.

Statistical analysis

No statistical methods were used to predetermine sample size. The significance of differences in the experimental data were determined using GraphPad Prism 7.0 software. All data involving statistics are presented as mean \pm s.e.m. For data presented without statistics, experiments were repeated at least three times to ensure reproducibility, unless otherwise stated. The experiments were not randomized, and investigators were not blinded to allocation during experiments and outcome assessment.

Reporting summary

Further information on research design is available in the Nature Research Reporting Summary linked to this paper.

Data availability

The ChIP-seq and RNA-seq data have been made available at the Gene Expression Omnibus (GEO) repository under the accession number GSE115354. The mass spectrometry proteomics data have been deposited to the ProteomeXchange Consortium via the PRIDE³¹ partner repository with the dataset identifier PXD014870. All other data are available from the authors upon reasonable request.

18. Kratz, M. et al. Metabolic dysfunction drives a mechanistically distinct proinflammatory phenotype in adipose tissue macrophages. *Cell Metab.* **20**, 614–625 (2014).
19. Shechter, D., Dormann, H. L., Allis, C. D. & Hake, S. B. Extraction, purification and analysis of histones. *Nat. Protocols* **2**, 1445–1457 (2007).
20. Cox, J. & Mann, M. MaxQuant enables high peptide identification rates, individualized p.p.b.-range mass accuracies and proteome-wide protein quantification. *Nat. Biotechnol.* **26**, 1367–1372 (2008).
21. Kim, D., Langmead, B. & Salzberg, S. L. HISAT: a fast spliced aligner with low memory requirements. *Nat. Methods* **12**, 357–360 (2015).
22. Robinson, M. D., McCarthy, D. J. & Smyth, G. K. edgeR: a Bioconductor package for differential expression analysis of digital gene expression data. *Bioinformatics* **26**, 139–140 (2010).
23. Huang, W., Sherman, B. T. & Lempicki, R. A. Systematic and integrative analysis of large gene lists using DAVID bioinformatics resources. *Nat. Protocols* **4**, 44–57 (2009).

24. Huang, W., Sherman, B. T. & Lempicki, R. A. Bioinformatics enrichment tools: paths toward the comprehensive functional analysis of large gene lists. *Nucleic Acids Res.* **37**, 1–13 (2009).
25. Cuddapah, S. et al. Native chromatin preparation and Illumina/Solexa library construction. *Cold Spring Harb. Protoc.* **2009**, pdb prot5237 (2009).
26. Langmead, B. & Salzberg, S. L. Fast gapped-read alignment with Bowtie 2. *Nat. Methods* **9**, 357–359 (2012).
27. Langmead, B., Trapnell, C., Pop, M. & Salzberg, S. L. Ultrafast and memory-efficient alignment of short DNA sequences to the human genome. *Genome Biol.* **10**, R25 (2009).
28. Li, H. et al. The Sequence Alignment/Map format and SAMtools. *Bioinformatics* **25**, 2078–2079 (2009).
29. Zhang, Y. et al. Model-based analysis of ChIP-Seq (MACS). *Genome Biol.* **9**, R137 (2008).
30. Liao, Y., Smyth, G. K. & Shi, W. featureCounts: an efficient general purpose program for assigning sequence reads to genomic features. *Bioinformatics* **30**, 923–930 (2014).
31. Perez-Riverol, Y. et al. The PRIDE database and related tools and resources in 2019: improving support for quantification data. *Nucleic Acids Res.* **47** (D1), D442–D450 (2019).

Acknowledgements HEK293T p300 knockout cells were provided by X. Li. We thank S. Khochbin for brainstorming and critical reading of this manuscript. We thank K. Delaney and all other members of the Zhao and Becker laboratories for discussions and technical support. This work was supported by the University of Chicago, Nancy and Leonard Florsheim family fund (Y.Z.), NIH grants R01GM15961, R01DK118266 (Y.Z.), R01DK102960, R01HL137998 (L.B.), R01CA129325, R01DK071900 (R.G.R.), and NSF1808087 (Y.G.Z.).

Author contributions Y.Z. conceived the project and developed the general ideas and research strategy. D.Z., L.B. and Y.Z. designed the experimental approach and composed the manuscript. D.Z. performed most of the experiments. Z.T. and R.G.R. carried out in vitro chromatin-based transcription experiments. Y.W., H.H., W.L., J.D., L.D., S.K., S.L. and M.P.-N. contributed to mass spectrometry-related experiments and analysis; R.H., Z.Y. and B.R. performed the library construction and next-generation sequencing for ChIP-seq and RNA-seq; M.H. and Y.G.Z. synthesized L-lactyl-CoA. H.H. and D.Z. analysed ChIP-seq and RNA-seq data. G.Z. provided all primary BMDM cell cultures. D.C. and H.A.S. carried out the bacterial infection experiments; C.C. carried out TAM experiments.

Competing interests Y.Z. is a co-founder, board member, and advisor to PTM Bio Inc. L.B. is a co-founder and CSO of rMark Bio Inc., and a founder and CEO of Oncilles Pharma Inc.

Additional information

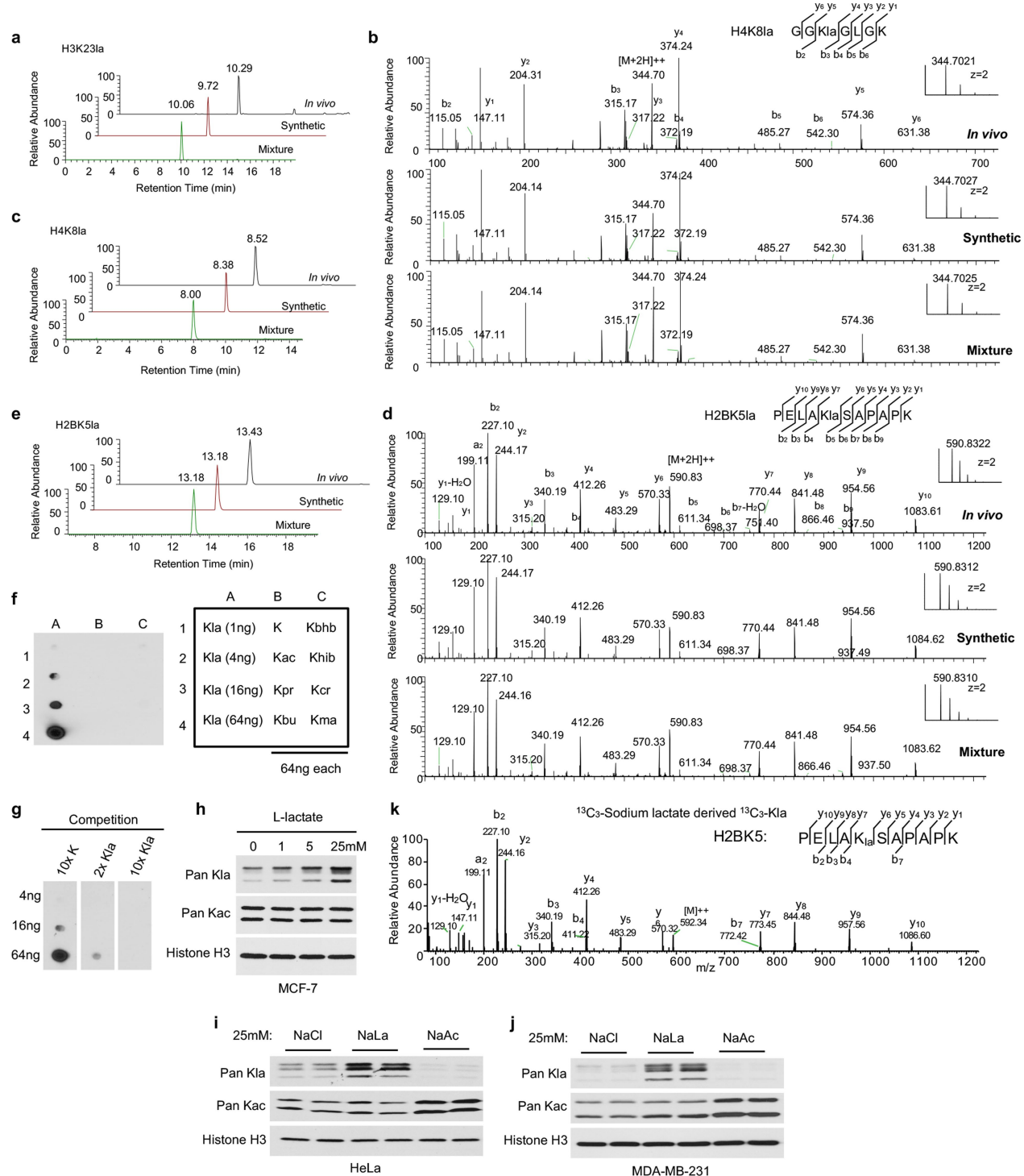
Supplementary information is available for this paper at <https://doi.org/10.1038/s41586-019-1678-1>.

Correspondence and requests for materials should be addressed to L.B. or Y.Z.

Peer review information *Nature* thanks Luke O'Neill, Kathryn Wellen and the other, anonymous, reviewer(s) for their contribution to the peer review of this work.

Reprints and permissions information is available at <http://www.nature.com/reprints>.

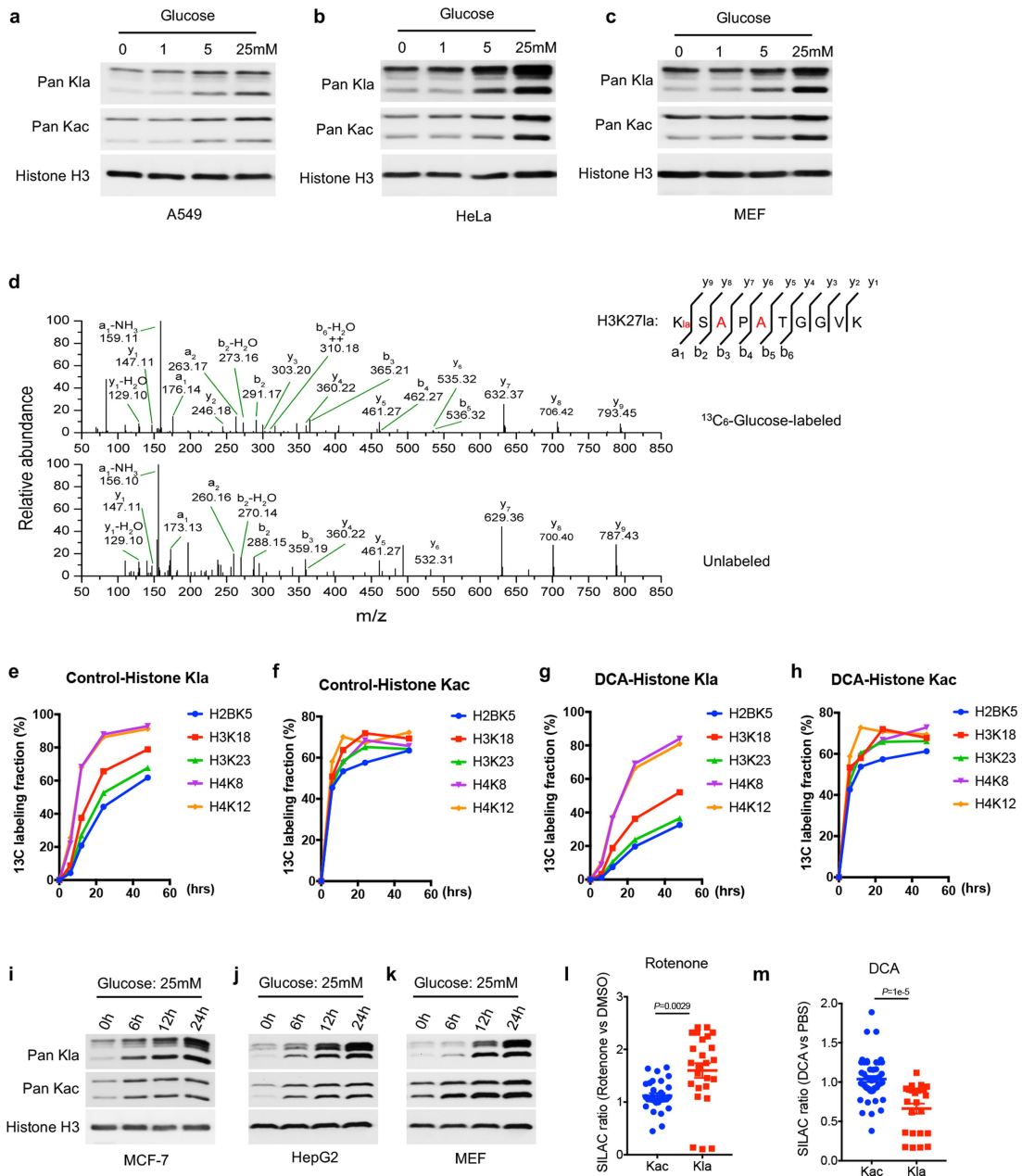
Article



Extended Data Fig. 1 | Validation of histone lysine lactylation.

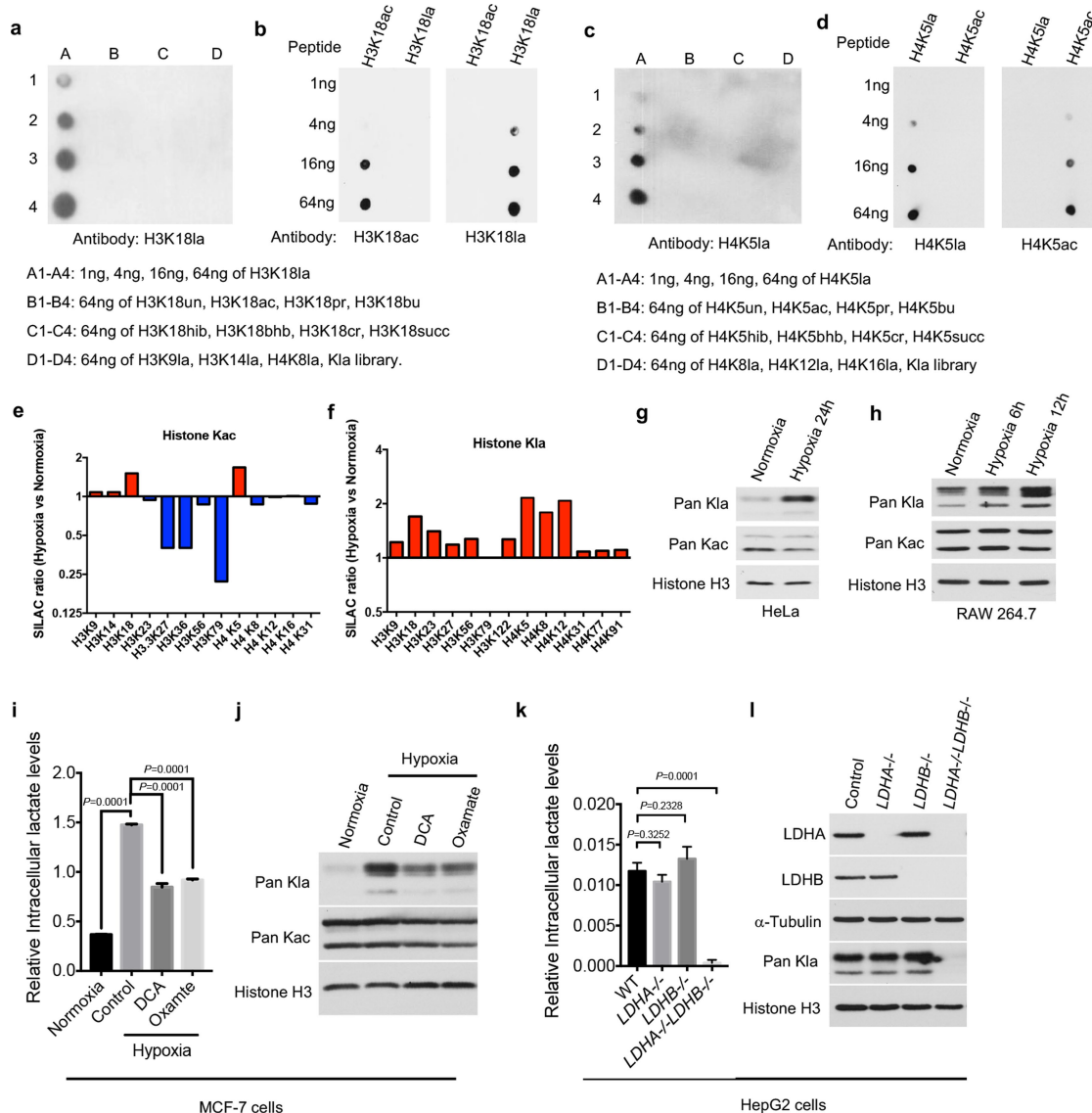
a, c, e. Extracted ion chromatograms from HPLC-MS/MS analysis of histone Kla peptides derived from cultured cells (*in vivo*), the synthetic counterparts, and their mixtures. **b, d.** MS/MS spectra of histone Kla peptides derived from *in vivo*, the synthetic counterparts, and their mixtures. **f, g.** Antibody specificity tests by dot blot and competition assay. **f.** Dot blot was carried out with a pan anti-Kla antibody and the following peptide libraries. A1, A2, A3 and A4: dots contain 1, 4, 16 and 64 ng, respectively, of a peptide library containing a lactylated lysine residue. B1, B2, B3 and B4: dots contain 64 ng of a peptide library containing an unmodified (K), acetylated (Kac), propionylated (Kpr) and butyrylated (Kbu) lysine residue, respectively. C1, C2, C3 and C4: dots contain 64 ng of a peptide library containing a β -hydroxybutyrylated (Kbhb), 2-hydroxyisobutyrylated

(Khib), crotonylated (Kcr) and malonylated (Kma) lysine residue, respectively. The libraries contained a mixture of CXXXKXXXX peptides, in which C is cysteine, X is a mixture of all 19 amino acids except for cysteine, and K is lysine with or without the indicated modifications. **g.** Competition was carried out by incubating the pan anti-Kla antibody with a twofold or tenfold excess of the indicated peptide libraries before the dot blot assay. **h–j.** Exogenous lactate boosts histone Kla levels. Immunoblot analysis of histone Kla and Kac from human MCF-7 cells treated with indicated doses of L-lactate (**h**), and from human HeLa (**i**) and MDA-MB-231 (**j**) cells treated with 25 mM sodium chloride, sodium lactate or sodium acetate. **k.** MS/MS spectra of an isotopically labelled histone Kla peptide identified from MCF-7 cells cultured with 10 mM isotopic ($^{13}\text{C}_3$) sodium L-lactate for 24 h. Data in **a–k** represent three independent experiments.



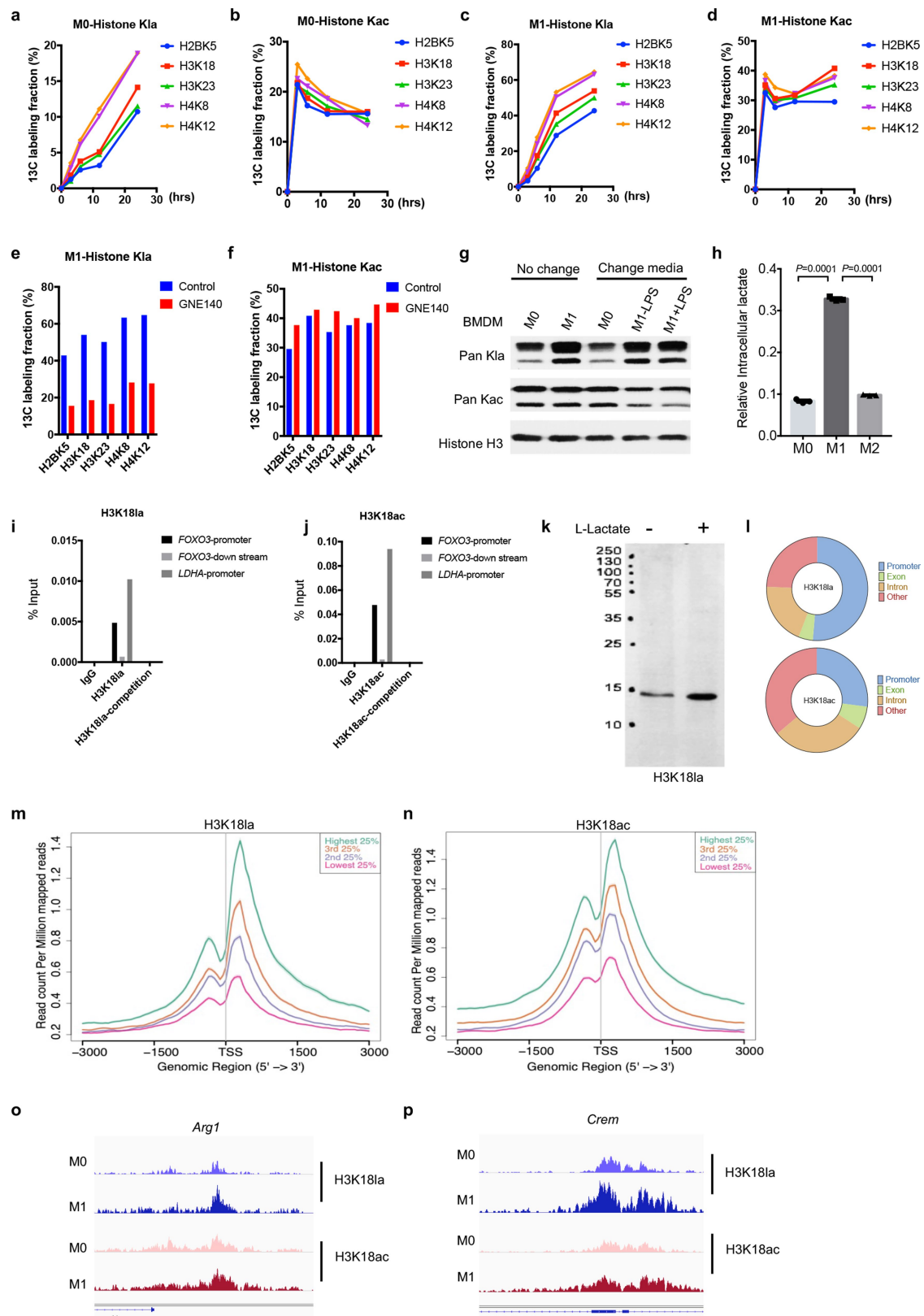
Extended Data Fig. 2 | Histone Kla is modulated by the glycolysis pathway.
a–c, A549 (**a**), HeLa (**b**) and mouse embryonic fibroblast (MEF) (**c**) cells were cultured with indicated doses of glucose for 24 h, without pyruvate. Histone Kla and Kac were analysed by immunoblots using indicated antibodies. **d**, MS/MS spectra of a U-¹³C₆-glucose labelled histone Kla peptide and its unlabelled counterpart from MCF-7 cells. **e–h**, Quantitative proteomic analysis of histone extracts from MCF-7 cells cultured in the presence of U-¹³C₆ glucose for 6 h, 12 h, 24 h and 48 h, with or without 10 mM DCA. **i–k**, Histone Kla and Kac levels were analysed by immunoblots using whole-cell lysates from MCF-7, HepG2 and MEF

cells exposed to 25 mM glucose for the indicated times. **l, m**, SILAC-MS/MS quantification of histone Kla and Kac marks from MCF-7 cells, comparing rotenone (10 nM, 24 h) versus DMSO treatment (**l**), and DCA (10 mM, 24 h) versus PBS treatment (**m**). SILAC ratio was normalized to protein abundance. Each dot in the scatter dot plot represents one identified peptide from core histone. Data are mean \pm s.e.m. **l**, Kac: 1.121 ± 0.05084 , $n = 31$; Kla: 1.599 ± 0.139 , $n = 25$. **m**, Kac: 1.038 ± 0.03813 , $n = 49$; Kla: 0.6627 ± 0.06376 , $n = 24$. Statistical significance was determined using two-tailed Welch's *t*-test. Data in **a–d, i–k** represent three independent experiments. Data in **e–h** represent two independent experiments.



Extended Data Fig. 3 | Histone Kla is induced by hypoxia. **a–d**, Antibody specificity was analysed by dot blot assay. ac, acetyl lysine; bhb, β -hydroxybutyryl lysine; bu, butyryl lysine; cr, crotonyl lysine; hib, 2-hydroxyisobutyryl lysine; la, lactyl lysine; pr, propionyl lysine; succ, succinyl lysine; un, unmodified lysine. Kla library contains a mixture of CXXXKlaXXXX peptides, in which C is cysteine, X is a mixture of all 19 amino acids except for cysteine, and Kla is lactyl lysine. **e,f**, SILAC-MS/MS quantification of histone Kla and Kac marks from MCF-7 cells, comparing hypoxic (1% oxygen for 24 h) and normoxic conditions. SILAC ratio was normalized to protein abundance. **g,h**, Immunoblots of histone Kla and Kac

from human HeLa and mouse RAW 264.7 cells in response to hypoxia (1% oxygen) at the indicated time. **i,j**, Intracellular lactate levels (**i**) and histone Kla levels (**j**) were measured in MCF-7 cells comparing normoxia, hypoxia (1% oxygen, 24 h) and hypoxia in the presence of 10 mM oxamate or DCA. **k,l**, Intracellular lactate levels (**k**) and histone Kla levels (**l**) were compared in LDHA^{-/-}, LDHB^{-/-}, LDHA^{-/-}/LDHB^{-/-} or wild-type (WT) HepG2 cells. Data are mean and s.e.m. from three biological independent samples; statistical significance was determined using one-way ANOVA followed by Dunnett's multiple comparisons test. Data in **a–d,g,h,k** and **l** represent three independent experiments.



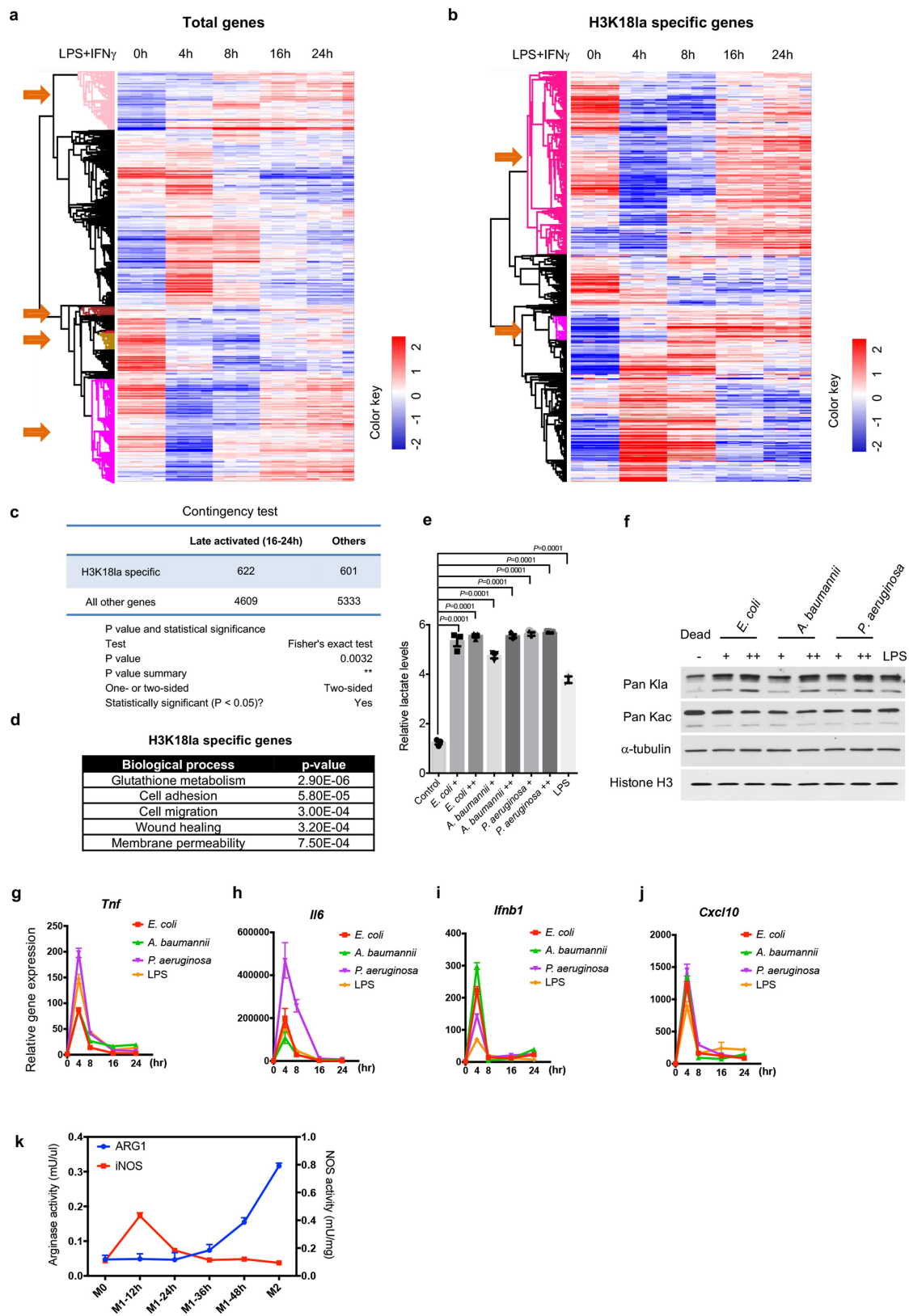
Extended Data Fig. 4 | See next page for caption.

Article

Extended Data Fig. 4 | Histone K1a is induced during M1 macrophage polarization.

a–f. Quantitative proteomic analysis of histone extracts from M0 and M1 macrophages (BMDMs) cultured in the presence of U-¹³C₆-glucose for 3, 6, 12 and 24 h, or with 10 µM GNE-140 (LDHA/B inhibitor) for 24 h. **g.** Histone K1a and Kac levels were analysed by immunoblots 24 h after activation by LPS and IFNγ, with or without replenishing fresh media (containing LPS and IFNγ or not) every 4 h. **h.** BMDM cells were stimulated with PBS (M0), LPS plus IFNγ (M1), and IL-4 (M2) for 24 h. Intracellular lactate was measured using a lactate colorimetric kit. Data are mean and s.e.m. from three biological independent samples; statistical significance was determined using one-way ANOVA followed by Dunnett's multiple comparisons test. **i,j.** Antibody specificity was evaluated by ChIP-qPCR. Competition was carried out by pre-incubating the indicated

antibodies with a tenfold excess of corresponding peptides. **k.** H3K18la antibody specificity was shown by full immunoblot using total lysate from MCF-7 cells with or without 10 mM sodium L-lactate treatment for 24 h. **l.** H3K18la and H3K18ac are enriched in promoter regions. The promoter was defined as regions ± 2 kb around known transcription start sites. **m,n.** H3K18la and H3K18ac correlate with steady-state mRNA levels. The average ChIP signal intensity (read count per million mapped reads) for indicated antibodies is shown for genes with different expression levels (the top 25%, the second 25%, the third 25%, and the bottom 25% of RNA-seq counts). **o,p.** IGV tracks for *Arg1* and *Crem* from ChIP-seq analysis, representing data from single experiment. Data in **a–f** represent two independent experiments. Data in **g,i–k** represent three independent experiments.

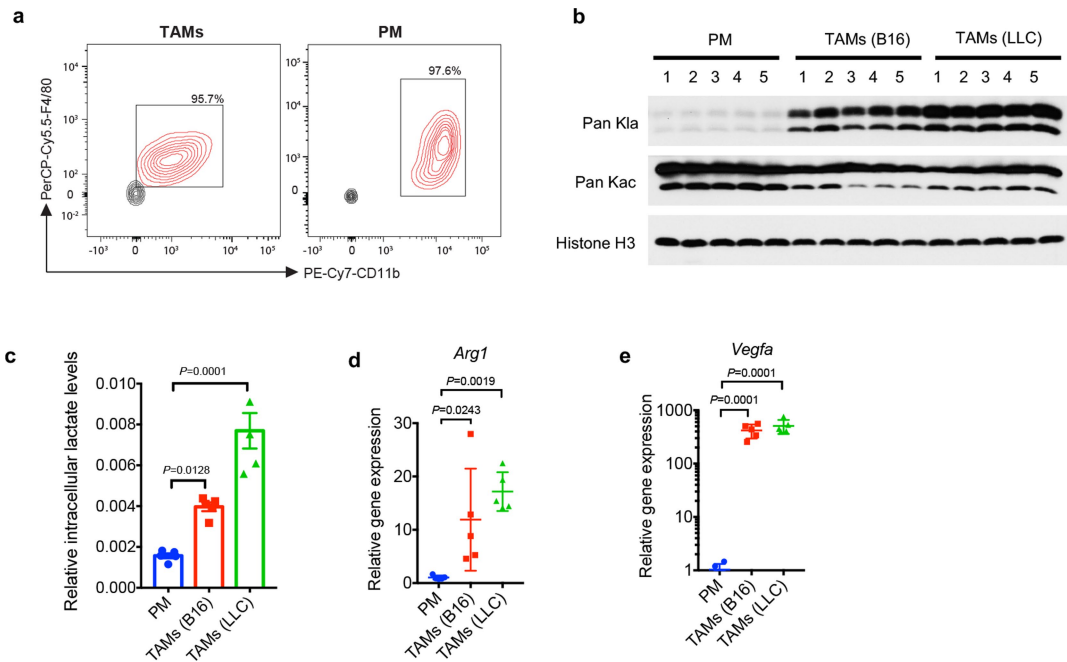


Extended Data Fig. 5 | See next page for caption.

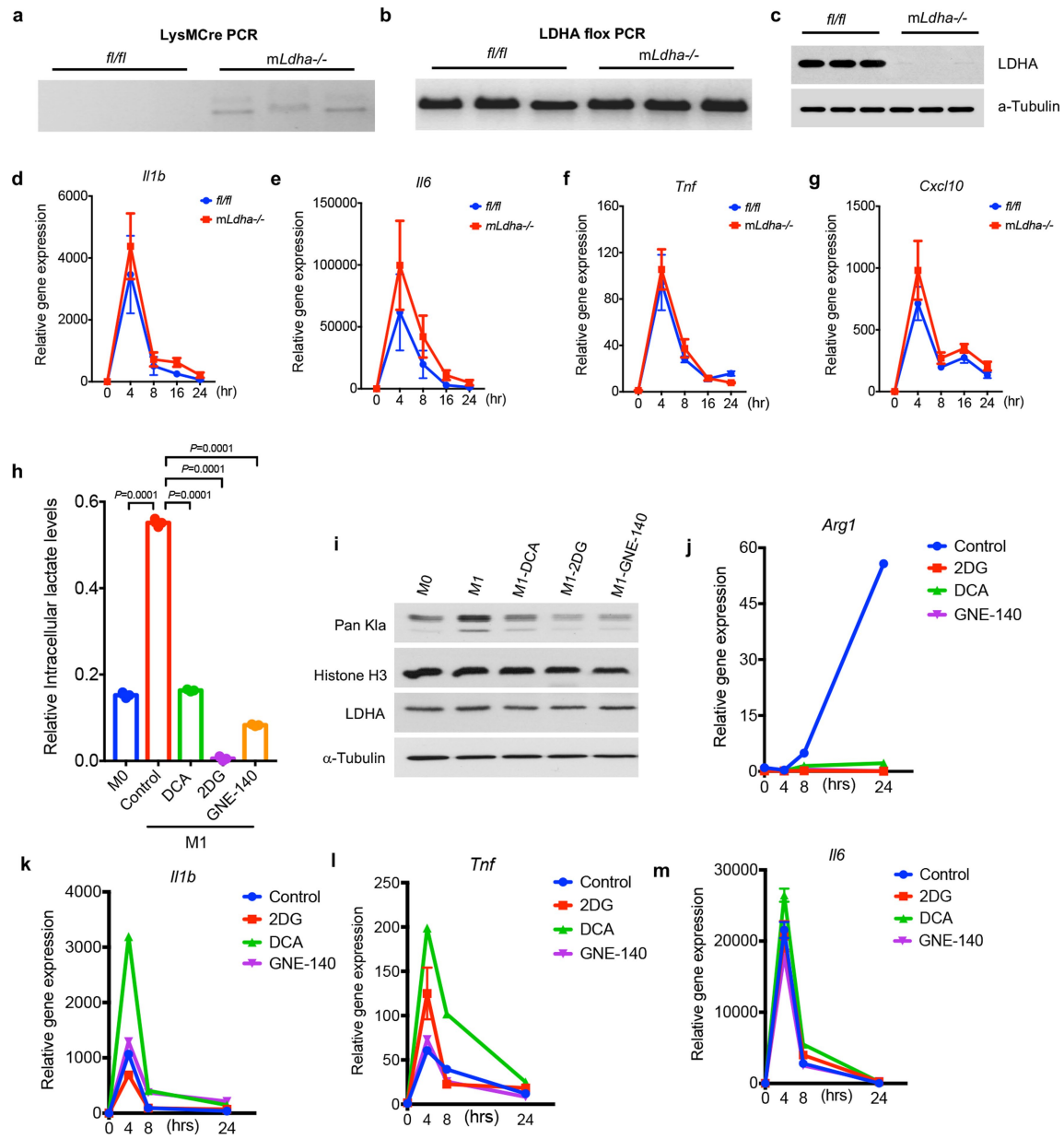
Article

Extended Data Fig. 5 | Histone Kla-specific genes are associated with late activated M2-like gene expression. **a, b,** Heat maps showing expression kinetics of total genes (**a**) and H3K18la-specific genes (**b**) during M1 macrophage polarization. $n = 4$ biological replicates. The colour key represents log₂-transformed fold change relative to the mean of each row. Arrows next to the heatmaps refer to late activated genes (16–24 h) from H3K18la-specific or total genes used for contingency test. **c,** Contingency table analysis (Fisher's exact tests) shows the relation between specific H3K18la enrichment (H3K18la log₂-transformed fold change ≥ 1 and H3K18ac log₂-transformed fold change ≤ 0.5) and late gene activation. **d,** Gene Ontology analysis (biological processes) of H3K18la-specific genes. Statistical significance was determined by modified

Fisher's exact test (EASE score) using DAVID bioinformatics resources 6.8; $n = 1,223$ genes. **e–j,** BMDM cells were infected with indicated Gram-negative bacteria for 24 h. Intracellular lactate (**e**) and histone Kla levels (**f**) were measured 24 h after bacterial challenge. **e, n = 3** biological replicates; statistical significance was determined using one-way ANOVA followed by Dunnett's multiple comparisons test. **g–j,** Gene expression was analysed by RT-qPCR at indicated time points after bacterial challenge. **k,** Activities of iNOS and ARG1 were analysed by commercialized kits from BMDMs activated by the indicated stimuli. Data are mean and s.e.m. from three biological replicates. Data in **f** and **k** represent three independent experiments.

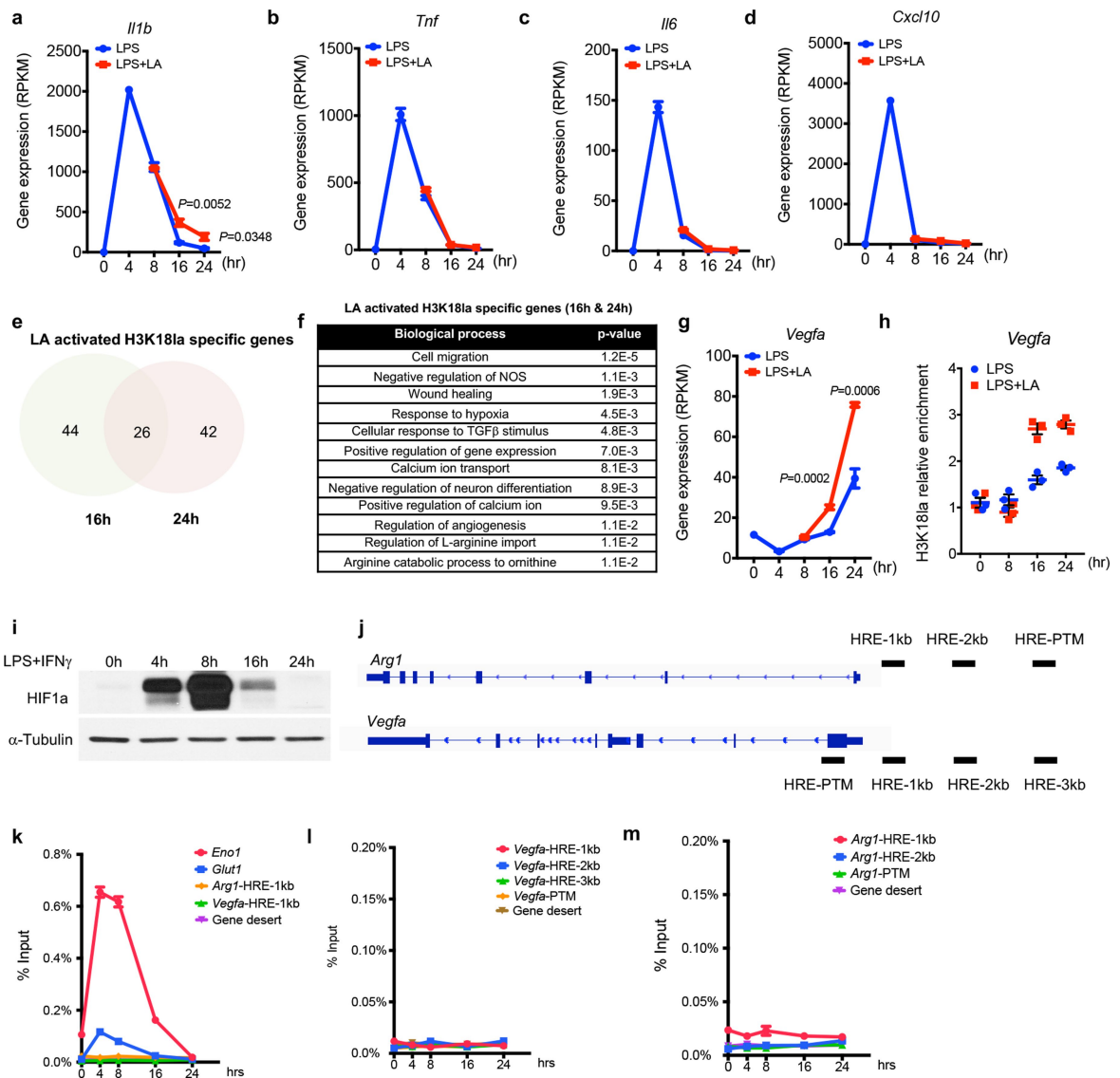


Extended Data Fig. 6 | Histone K1a levels are positively correlated with Arg1 expression in TAMs. **a**, The purity of TAMs and peritoneal macrophages (PMs) was confirmed by flow cytometry using CD11b and F4/80 antibodies. **b–e**, Data were quantified by FlowJo v10.4.1. Histone K1a and Kac levels were analysed by immunoblots (**b**), intracellular lactate was measured using a lactate colorimetric assay kit (**c**), and gene expression of *Arg1* and *Vegfa* were analysed by RT-qPCR



Extended Data Fig. 7 | Decreased lactate production lowered histone Kla levels and Arg1 expression during M1 polarization. **a, b**, Genotyping of *Ldha*^{fl/fl} × LysM-Cre^{+/−} mice. **c**, Genotype validation by LDHA immunoblot analysis. **d–g**, Gene expression analysis of cytokines by RT-qPCR at indicated time points after M1 polarization. **h–m**, Intracellular lactate levels (**h**) were analysed using a lactate colorimetric assay kit and global histone Kla levels (**i**)

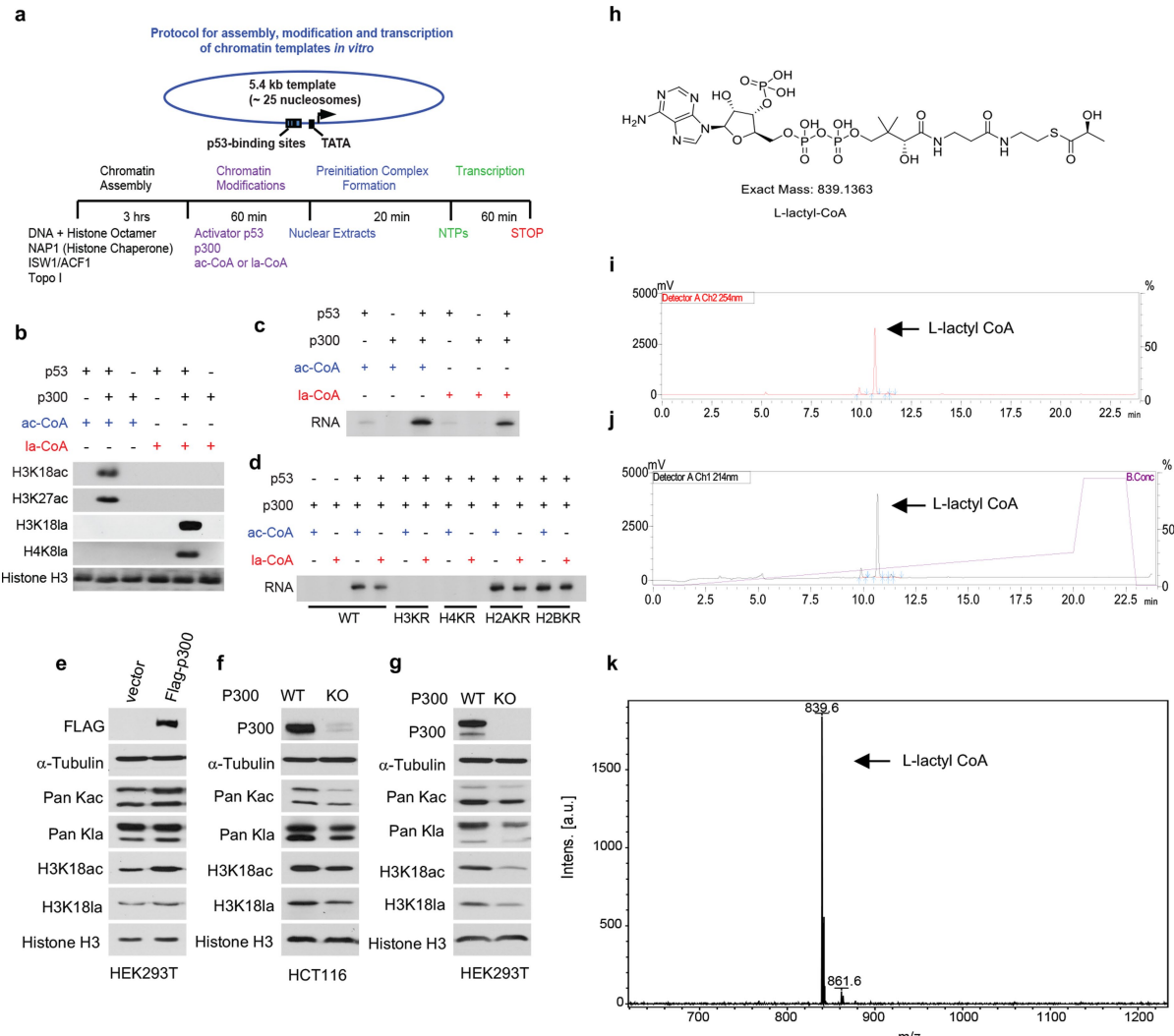
were measured by immunoblots 24 h after M1 polarization. Inhibitors were treated 30 min after M1 polarization. Gene expression was analysed by RT-qPCR at indicated time points after M1 polarization (**j–m**). Data are mean and s.e.m. from three biological replicates. Statistical significance was determined using one-way ANOVA followed by Dunnett's multiple comparisons test. Data in **a–c** and **i** represent three independent experiments.



Extended Data Fig. 8 | Exogenous lactate activates M2-like gene expression through histone Kla. **a–d**, Exogenous lactate (LA) does not interfere with gene expression of inflammatory cytokines. Data are mean \pm s.e.m. from four biological replicates. **e**, Number of lactate-activated H3K18la-specific genes at indicated times are shown in a Venn diagram. **f**, Gene Ontology analysis (biological processes) of lactate-induced H3K18la-specific genes at 16 and 24 h after M1 polarization. Statistical significance was determined by modified Fisher's exact test (EASE score) using DAVID bioinformatics resources 6.8; $n=112$ genes. **g**, *Vegfa* was induced by exogenous lactate during M1 macrophage polarization; $n=4$ biological replicates; statistical significance was determined

using multiple *t*-tests corrected using the Holm–Sidak method. **h**, H3K18la occupancy at the *Vegfa* promoter was analysed by ChIP–qPCR at indicated time and treatment; data represent three technical replicates from pooled samples. **i–m**, HIF1a is not required for histone Kla-mediated *Arg1* induction during M1 polarization. **i**, Immunoblot of HIF1a at indicated time points after M1 polarization. **j**, Illustration of genomic loci targeted by *Arg1* and *Vegfa* ChIP–qPCR primers. HRE indicates regions containing the putative HIF1a binding motif 'ACGTG'. **k–m**, ChIP–qPCR analysis of HIF1a binding to indicated genomic locations; data represent three technical replicates from pooled samples. Data are mean and s.e.m. Data in **i** represent three independent experiments.

Article



Extended Data Fig. 9 | Histone Kla directly stimulates gene transcription from recombinant chromatin *in vitro*. **a**, Protocol for assembly, modification and transcription of chromatin templates. **b**, P300 catalyses histone lactylation in a p53-dependent manner. **c**, Histone lactylation directly stimulates p53-dependent transcription from recombinant chromatin. **d**, H3 and H4 lysine-to-arginine (KR) mutations eliminate p300-dependent transcriptional activation by p53. Recombinant chromatin was assembled with wild-type or H3KR, H4KR, H2AKR or H2BKR mutant histones as indicated. **e**, HEK293T cells were

transfected with vector or Flag-tagged p300 plasmid. At 48 h after transfection, whole-cell lysates were prepared and immunoblotted with indicated antibodies. **f,g**, Immunoblots of histone Kla and Kac levels in HCT116 (**f**) and HEK293T cells (**g**) in which p300 was genetically deleted. **h–k**, Quality control of synthesized L-lactyl-CoA. **h**, Illustration of L-lactyl-CoA structure. **i,j**, HPLC analysis of the synthesized L-lactyl-CoA. The UV detection wavelength was fixed at 214 and 254 nm. **k**, MALDI-mass spectrometry analysis of L-lactyl-CoA. Data in **b–g** and **i–k** represent three independent experiments.

Reporting Summary

Nature Research wishes to improve the reproducibility of the work that we publish. This form provides structure for consistency and transparency in reporting. For further information on Nature Research policies, see [Authors & Referees](#) and the [Editorial Policy Checklist](#).

Statistics

For all statistical analyses, confirm that the following items are present in the figure legend, table legend, main text, or Methods section.

n/a Confirmed

- The exact sample size (n) for each experimental group/condition, given as a discrete number and unit of measurement
- A statement on whether measurements were taken from distinct samples or whether the same sample was measured repeatedly
- The statistical test(s) used AND whether they are one- or two-sided
Only common tests should be described solely by name; describe more complex techniques in the Methods section.
- A description of all covariates tested
- A description of any assumptions or corrections, such as tests of normality and adjustment for multiple comparisons
- A full description of the statistical parameters including central tendency (e.g. means) or other basic estimates (e.g. regression coefficient) AND variation (e.g. standard deviation) or associated estimates of uncertainty (e.g. confidence intervals)
- For null hypothesis testing, the test statistic (e.g. F , t , r) with confidence intervals, effect sizes, degrees of freedom and P value noted
Give P values as exact values whenever suitable.
- For Bayesian analysis, information on the choice of priors and Markov chain Monte Carlo settings
- For hierarchical and complex designs, identification of the appropriate level for tests and full reporting of outcomes
- Estimates of effect sizes (e.g. Cohen's d , Pearson's r), indicating how they were calculated

Our web collection on [statistics for biologists](#) contains articles on many of the points above.

Software and code

Policy information about [availability of computer code](#)

Data collection

Mass spectrometry: Thermo Xcalibur 3.0.63
Flow cytometry: FACSDiva 10.5.3

Data analysis

GraphPad 7.0 was used to perform general statistical analyses.
ChIP-seq and RNAseq:
FastQC version 0.11.4, Bowtie version 2.2.6, SAMtools version 0.1.19, MACS version 2.2.1, featureCounts version 1.5.0-p1, DAVID Bioinformatics Resources 6.8, HISAT2 version 2.1.0, edgeR version 3.16.5, and Perseus version 1.6.1.1.
Mass spectrometry: MaxQuant 1.3.0.5.
Flow Cytometry: FlowJo v.10.4.1.

For manuscripts utilizing custom algorithms or software that are central to the research but not yet described in published literature, software must be made available to editors/reviewers. We strongly encourage code deposition in a community repository (e.g. GitHub). See the Nature Research [guidelines for submitting code & software](#) for further information.

Data

Policy information about [availability of data](#)

All manuscripts must include a [data availability statement](#). This statement should provide the following information, where applicable:

- Accession codes, unique identifiers, or web links for publicly available datasets
- A list of figures that have associated raw data
- A description of any restrictions on data availability

The ChIP-seq and RNA-seq data have been made available at the Gene Expression Omnibus (GEO) repository under the accession number GSE115354. All other data are available from the authors upon reasonable request.

Field-specific reporting

Please select the one below that is the best fit for your research. If you are not sure, read the appropriate sections before making your selection.

- Life sciences Behavioural & social sciences Ecological, evolutionary & environmental sciences

For a reference copy of the document with all sections, see nature.com/documents/nr-reporting-summary-flat.pdf

Life sciences study design

All studies must disclose on these points even when the disclosure is negative.

Sample size	Specific sample sizes are described in figures or figure legends for all experiments. The sample size used for animal experiment is based on previous experience from the Zhao and Becker labs. No statistical test was used to pre-determine sample size.
Data exclusions	No samples or animals were excluded from the analyses.
Replication	The number of repeats for each experiments are described in corresponding figure legends. All repeats support the same conclusion.
Randomization	Cells or mice tissue were randomly assigned to groups (chemical compound/hypoxia/other treatments).
Blinding	For animal related experiments, the investigators were divided into two groups: one group is responsible for collecting samples and the other group is responsible for experiment and outcome assessment.

Reporting for specific materials, systems and methods

We require information from authors about some types of materials, experimental systems and methods used in many studies. Here, indicate whether each material, system or method listed is relevant to your study. If you are not sure if a list item applies to your research, read the appropriate section before selecting a response.

Materials & experimental systems		Methods	
n/a	Involved in the study	n/a	Involved in the study
<input type="checkbox"/>	<input checked="" type="checkbox"/> Antibodies	<input type="checkbox"/>	<input checked="" type="checkbox"/> ChIP-seq
<input type="checkbox"/>	<input checked="" type="checkbox"/> Eukaryotic cell lines	<input type="checkbox"/>	<input checked="" type="checkbox"/> Flow cytometry
<input checked="" type="checkbox"/>	<input type="checkbox"/> Palaeontology	<input checked="" type="checkbox"/>	<input type="checkbox"/> MRI-based neuroimaging
<input type="checkbox"/>	<input checked="" type="checkbox"/> Animals and other organisms		
<input checked="" type="checkbox"/>	<input type="checkbox"/> Human research participants		
<input checked="" type="checkbox"/>	<input type="checkbox"/> Clinical data		

Antibodies

Antibodies used	<p>The following antibodies were generated by PTM Bio Inc (Chicago, IL):</p> <p>pan anti-Kac (PTM-101), 1:2000 (WB)</p> <p>pan anti-Kla (PTM-1401), 1:2000 (WB)</p> <p>anti-H3K18la (PTM-1406), 1:5000 (WB), 4ug per per ChIP</p> <p>anti-H4K8la (PTM-1405), 1:5000 (WB)</p> <p>anti-H4K5la (PTM-1407), 1:5000 (WB)</p> <p>The following antibodies were generated by Abcam (Cambridge, MA):</p> <p>anti-histone H3 (ab12079), 1:10000(WB)</p> <p>anti-H3K18ac (ab1191), 1:10000 (WB), 4ug per ChIP</p> <p>anti-H3K27ac (ab4729), 1:5000 (WB)</p> <p>The following antibodies were generated by Active Motif (Carlsbad, CA):</p> <p>anti-drosophila spike-in antibody (61686), 2ug per ChIP</p> <p>The following antibodies were generated by Cell Signaling Technology (Danvers, MA):</p> <p>anti-LDHA (2012S), 1:2000 (WB)</p> <p>The following antibodies were generated by Millipore Sigma (Burlington, MA):</p> <p>anti-a-Tubulin (05-829), 1:5000 (WB)</p> <p>anti-LDHB (ABC927), 1:2000 (WB)</p>
-----------------	---

The following antibodies were generated by Novus Biologicals (Littleton, CO):
anti-HIF-1α (NB100-105), 1:2000 (WB)

The following antibodies were generated by GeneTex (Irvine, CA):
anti-iNOS (GTX130246), 1:2000 (WB)
anti-Arg1 (GTX109242), 1:2000 (WB)

The following antibodies were generated by Santa Cruz Biotechnology, Inc (Dallas, TX):
anti-p300 (sc-584), 1:2000 (WB)

The following antibodies were generated by ThermoFisher Scientific (Waltham, MA):
anti-CD11b Monoclonal Antibody (M1/70), PE-Cyanine7, eBioscience (25-0112-82), 0.125 µg/test (Flow)
anti-F4/80 Monoclonal Antibody (BM8), APC, eBioscience (17-4801-82), 2 µg/test (Flow)

The following antibodies were generated by Jackson ImmunoResearch Laboratories (West Grove, PA):
Peroxidase AffiniPure Goat Anti-Mouse IgG (H+L) (115-035-003), 1:10000 (WB)
Peroxidase AffiniPure Goat Anti-Rabbit IgG (H+L) (111-035-003), 1:10000 (WB)

Validation

Pan anti-Kac (PTM-101):

Species: human, mouse; Application: Western Blot, Immunoprecipitation; Manufacturer's web site: <https://www.ptmbiolabs.com/product/ptm-101/>

Pan anti-Kla (PTM-1401):

Species: human, mouse; Application: Dot Blot, Western Blot, Immunoprecipitation; Validated in this paper.

Anti-H4K8la (PTM-1405):

Species: human, mouse; Application: Western Blot; Validated in this paper.

Anti-H3K18la (PTM-1406):

Species: human, mouse; Application: Dot Blot, Western Blot, ChIP; Validated in this paper.

Anti-H4K5la (PTM-1407):

Species: human, mouse; Application: Dot Blot, Western Blot; Validated in this paper.

Anti-histone H3 (ab12079):

Species: human, mouse; Application: Western Blot; Manufacturer's web site: <https://www.abcam.com/histone-h3-antibody-chip-grade-ab12079.html>

Anti-H3K18ac (ab1191):

Species: human, mouse; Application: Western Blot, ChIP; Manufacturer's web site: <https://www.abcam.com/histone-h3-acetyl-k18-antibody-chip-grade-ab1191.html>

Anti-H3K27ac (ab4729):

Species: human, mouse; Application: Western Blot; Manufacturer's web site: <https://www.abcam.com/histone-h3-acetyl-k27-antibody-chip-grade-ab4729.html>

Anti-LDHA (2012S):

Species: human, mouse; Application: Western Blot; Manufacturer's web site: <https://www.cellsignal.com/products/primary-antibodies/ldha-antibody/2012>

Anti-α-Tubulin (05-829):

Species: human, mouse; Application: Western Blot; Manufacturer's web site: https://www.emdmillipore.com/US/en/product/Anti-Tubulin-Antibody-clone-DM1A,MM_NF-05-829

Anti-LDHB (ABC927):

Species: human, mouse; Application: Western Blot; Manufacturer's web site: https://www.emdmillipore.com/US/en/product/Anti-LDHB-Antibody,MM_NF-ABC927

Anti-drosophila spike-in antibody (61686):

Species: drosophila; Application: ChIP; Manufacturer's web site: <https://www.activemotif.com/catalog/1091/chip-normalization>

Anti-iNOS (GTX130246):

Species: mouse; Application: Western Blot; Manufacturer's web site: <https://www.genetex.com/Product/Detail/iNOS-antibody/GTX130246>

Anti-Arg1(GTX109242):

Species: mouse; Application: Western Blot; Manufacturer's web site: <https://www.genetex.com/Product/Detail/Arginase-1-antibody/GTX109242>

anti-p300 (N15) (sc-584):

Species: human; Application: Western Blot; Manufacturer's web site: <https://www.scbt.com/scbt/product/p300-antibody-n-15> p300 (N-15) has been discontinued and replaced by p300 (F-4): sc-48343.

Anti-CD11b Monoclonal Antibody (M1/70), PE-Cyanine7, eBioscience (25-0112-82):
 Species: mouse; Application: Flow cytometry; Manufacturer's web site: <https://www.thermofisher.com/antibody/product/CD11b-Antibody-clone-M1-70-Monoclonal/25-0112-82>

Anti-F4/80 Monoclonal Antibody (BM8), APC, eBioscience (17-4801-82),
 Species: mouse; Application: Flow cytometry; Manufacturer's web site: <https://www.thermofisher.com/antibody/product/F4-80-Antibody-clone-BM8-Monoclonal/17-4801-82>

Eukaryotic cell lines

Policy information about [cell lines](#)

Cell line source(s)	HeLa, MCF-7, A549, MDA-MB-231, HepG2, MEF, and RAW264.7 cells were obtained from the American Type Culture Collection.
Authentication	HeLa, MCF-7, A549, MDA-MB-231, HepG2, MEF, and RAW264.7 cells were authenticated based on our vast experience working with these cell lines (such as cell morphology, culture conditions, etc.). Furthermore, we believe that the modification we described in the paper is widely existed in various cell lines, not specific to certain cell types.
Mycoplasma contamination	Cells were routinely tested for mycoplasma contamination, and only negative cells were used in experiments
Commonly misidentified lines (See ICLAC register)	None of the cell lines used are listed in the database of commonly misidentified cell lines maintained by ICLAC.

Animals and other organisms

Policy information about [studies involving animals](#); [ARRIVE guidelines](#) recommended for reporting animal research

Laboratory animals	Adult male mice (<i>Mus musculus</i> , C57BL/6, 7-10 weeks old) were purchased from The Jackson Laboratory, and were used to generate bone marrow derived macrophages (BMDMs). Ldhaf1/fl mice (Jackson laboratory, 030112) and LysMcre mice (Jackson laboratory, 004781) were used to generate LysMcre+/- Ldhaf1/fl and littermate control LysM-cre-/- Ldhaf1/fl mice.
Wild animals	The study did not involve samples collected from wild animals.
Field-collected samples	The study did not involve samples collected from the field.
Ethics oversight	All animal protocols were approved by Institutional Animal Care and Use Committee (ACUP) at the University of Chicago.

Note that full information on the approval of the study protocol must also be provided in the manuscript.

ChIP-seq

Data deposition

- Confirm that both raw and final processed data have been deposited in a public database such as [GEO](#).
- Confirm that you have deposited or provided access to graph files (e.g. BED files) for the called peaks.

Data access links <small>May remain private before publication.</small>	https://www.ncbi.nlm.nih.gov/geo/query/acc.cgi?acc=GSE115354
Files in database submission	GSM3176446_RH_148_peaks.broadPeak.gz GSM3176447_RH_229_peaks.broadPeak.gz GSM3176449_RH_151_peaks.broadPeak.gz GSM3176450_RH_231_peaks.broadPeak.gz GSE115354_ChIP-seq_normalization.txt.gz
Genome browser session (e.g. UCSC)	N/A

Methodology

Replicates	ChIP-seq samples are prepared as one replicate, pooled from four mice
Sequencing depth	RH_148 (unique reads: 21765076; spike-in reads: 310066) RH_151 (unique reads: 21006731; spike-in reads: 141688) RH_229 (unique reads: 36576826; spike-in reads: 52482) RH_231 (unique reads: 32948615; spike-in reads: 50470)
Antibodies	The anti-H3K18la antibody was generated by PTM biolabs. The process for generating antibodies were described similarly in Cell, 2011. 146: p. 1016-1028. Mol Cell, 2015. 58(2): p. 203-15. Nat Chem Biol, 2014. 10(5): p. 365-70. except for using different immunogens. The anti-H3K18ac antibody was purchased from Abcam(ab1191, lot GR 300534-1)

The evaluation of the antibody for specificity and ChIP grade is provided in the manuscript.
 Spike-in information: spike-in chromatin (Active motif, Catalog No. 53083), spike-in antibody (Active motif, Catalog No. 61686)

Peak calling parameters

Peaks were called using MACS version 2.2.1 under q value = 0.01.

Data quality

Sequencing quality was evaluated by FastQC version 0.11.4. All reads were mapped to reference genome of illumina iGenomes UCSC mm10 using Bowtie version 2.2.6, and only uniquely mapped reads were retained. SAMtools version 0.1.1926 was used to convert files to bam format, sort, and remove PCR duplicates. Peaks were called using MACS version 2.2.1 under q value = 0.01.
 The number of peaks at the cutoff threshold in each sample:
 21885 peaks in GSM3176446_RH_148_peaks.broadPeak.gz
 41493 peaks in GSM3176447_RH_229_peaks.broadPeak.gz
 16139 peaks in GSM3176449_RH_151_peaks.broadPeak.gz
 42237 peaks in GSM3176450_RH_231_peaks.broadPeak.gz

Software

Base called by Real-Time Analysis (RTA)
 Reads were mapped to reference genome of illumina iGenomes UCSC mm10 using Bowtie version 2.2.6, and only uniquely mapped reads were retained.
 SAMtools version 0.1.19 was used to convert files to bam format, sort, and remove PCR duplicates.
 Peaks were called using MACS version 2.2.1 under q value = 0.01.
 Uniquely mapped reads of each gene were counted by featureCounts version 1.5.0-p1, and normalized by corresponding uniquely mapped spiked-in ChIP read counts.

Flow Cytometry

Plots

Confirm that:

- The axis labels state the marker and fluorochrome used (e.g. CD4-FITC).
- The axis scales are clearly visible. Include numbers along axes only for bottom left plot of group (a 'group' is an analysis of identical markers).
- All plots are contour plots with outliers or pseudocolor plots.
- A numerical value for number of cells or percentage (with statistics) is provided.

Methodology

Sample preparation

0.2 million cells were labeling with different fluorophore conjugated antibody at room temperature for 15mins, followed by two washes.

Instrument

Samples were analyzed using a FACSCanto™ II flow cytometer.

Software

Data were quantified by FlowJo v.10.4.1.

Cell population abundance

Purity for both TAM and Pmac are above 95% based on F4/80 and CD11b cell surface marker. positive gating were determined by negative control.

Gating strategy

Cells were gated by FSC/SSC for total population --> SSC-A/SSC-H for single cells --> cblue labeling for live cells population --> F4/80 and CD11b double positive (compared to negative population) for purity check.

Tick this box to confirm that a figure exemplifying the gating strategy is provided in the Supplementary Information.